SELECTIVELY ERBIUM DOPED TITANIUM DIFFUSED OPTICAL WAVEGUIDE AMPLIFIERS IN LITHIUM NIOBATE

A Thesis

by

JAE WOO SUH

Submitted to the Office of Graduate Studies of
Texas A&M University
in partial fulfillment of the requirements for the degree of

MASTER OF SCIENCE

December 2010

Major Subject: Electrical Engineering

SELECTIVELY ERBIUM DOPED TITANIUM DIFFUSED OPTICAL WAVEGUIDE AMPLIFIERS IN LITHIUM NIOBATE

A Thesis

by

JAE WOO SUH

Submitted to the Office of Graduate Studies of
Texas A&M University
in partial fulfillment of the requirements for the degree of

MASTER OF SCIENCE

Approved by :

Chair of Committee,	Ohannes Eknoyan
Committee Members,	Chanan Singh
	Christi Madsen
	Lewis Ntaimo
Head of Department,	Costas N. Georghiades

December 2010

Major Subject: Electrical Engineering

ABSTRACT

Selectively Erbium Doped Titanium Diffused Optical

Waveguide Amplifiers in Lithium Niobate.

(December 2010)

Jae Woo Suh, B.S., Texas A&M University

Chair of Advisory Committee: Dr. Ohannes Eknoyan

Selectively erbium (Er) doped titanium (Ti) in-diffused optical waveguide amplifiers on lithium niobate ($LiNbO_3$) substrate have been fabricated and characterized in the wavelength regime around $\lambda = 1.53\mu m$ using counter-directional pumping at $\lambda_P = 1.48\mu m$. $LiNbO_3$ waveguide amplifiers are desirable for providing gain in optical circuit chips through integration with other optical elements on a single substrate. A prerequisite for achieving useful gain rests on the optimization of overlap between the incident guided optical signal mode distribution and the evolving emission from excited Er ions. The extent of overlap can be controlled by adjusting fabrication parameters.

Fabrication parameters for Er-doped Ti in-diffused waveguide amplifiers of useful optical gain have been optimized by diffusing selective patterns of vacuum-deposited 17nm-thick erbium film at 1100˚C for 100 hours into $LiNbO_3$, and integrating with 7μm-wide single mode straight channel waveguides formed by diffusing 1070Å thick titanium film into the $LiNbO_3$. Small-signal gain characterization was carried out with a -30 dBm of transmitted input signal power at λ_S=1531nm with counter-

directionally launched pump power ranging between 0 to 119mW at λ_P=1488nm, using TM polarization for both the signal and pump beams. At a maximum launched pump power of 119mW, a signal enhancement of 8.8dBm for 25mm-long erbium doped region, and 11.6dBm for 35mm-long erbium doped region were obtained. The corresponding calculated net gain values are 1.8dB and 2.8dB, for the 25mm-long and 35mm-long Er-doped regions, respectively.

To My Family

ACKNOWLEDGEMENTS

I would like to thank my advisor and committee chair, Dr. Ohannes Eknoyan, for his advice, guidance and support during my M.S. program at Texas A&M University. His careful approach and pursuit of perfection on the research work deserve sincerely deep respect. Without his precious support and instruction, this thesis would not be completed. Also, I appreciate Dr. Christi Madsen, Dr. Chanan Singh and Dr. Lewis Ntaimo for serving as members of my committee. I truly thank Mr. Robert Atkins, Mr. Jim Gardner and Mr. Dennie Spears for their technical training, support and collaboration for my entire research work in the lab. I would like to express my gratitude to Renato Rabelo, Yongwook Shin, Jaewon Park, Hyunsoo Kim, Wonju Sung, Wee Chong Tan and KASA members for their advice, support and friendship.

Finally, I would like to most warmly thank to my parents, my brother, my lovely wife HeiJoung Kim, my baby and the Lord who gives my baby a precious life.

TABLE OF CONTENTS

Page

TABLE OF CONTENTS (continued)

Page

LIST OF FIGURES

LIST OF FIGURES (continued)

LIST OF TABLES

CHAPTER I

INTRODUCTION

For applications in optical communication systems and networks, rare-earth doped optically-pumped waveguide amplifier devices in a planar substrate such as $LiNbO_3$ have attracted great interests because they can provide highly achievable gain and low noise at particular useful wavelength regimes. This makes it possible to compensate for scattering, absorption, and insertion losses, even to provide optical gain or lasing. Specifically, erbium doped devices operate in the wavelength range near λ = 1.5μm which is the wavelength regime used in optical communications. As such, merging the erbium emission properties with those of devices on $LiNbO_3$ substrate has attracted considerable interest because it enables the interaction of optically active erbium ions with the excellent electro-optical and acousto-optical properties of $LiNbO_3$ [1]. Furthermore, combining optical amplifiers with other active and passive devices on a single substrate also allows making integrated optical circuits (IOC's) for a variety of other optical applications including sensing, signal processing and measurement techniques [2].

To optimize the performance of the optical amplifier, it is essential to have a good description of the evolution of the signal, pump and fluorescence powers in the active region [2]. Furthermore, to ascertain the combination between erbium and $LiNbO_3$,

---

This thesis follows the style and format of *IEEE Journal of Lightwave Technology*.

it is very important to know the spectral characteristics of the dopant-host combination and to quantify radiative and non-radiative transitions between different excited levels [3].

Recent research activities at Texas A&M University have demonstrated an erbium doped titanium diffused lithium niobate ($LiNbO_3$) waveguide amplifier for Transverse Magnetic (TM) polarization in the 1.55μm wavelength regime. The critical points of the device to have best performance and repeatability are proper erbium doping into the substrate, and well-confined overlap between the erbium doped region and the signal/pump modes distribution within the titanium in-diffused channel waveguide.

Erbium doped waveguide amplifiers (EDWAs) have been demonstrated using two doping techniques: homogeneous bulk doping or selective surface doping. Homogeneous doping can be realized during crystal growth from an erbium doped melt [4]. However, it is difficult to achieve high-quality striation-free crystals of high doping concentration and large size [5]. On the other hand, Er-doping of a surface layer can be realized by implantation and annealing [6] or by in-diffusion of a vacuum-deposited Er-film [7], [8]. For this research, the in-diffusion doping method is used.

The purpose of the research is to develop optimized processes for fabricating and realizing repeatable maximum-achievable optical gain in erbium (Er) doped titanium (Ti) in-diffused lithium niobate ($LiNbO_3$) waveguide amplifier around at the 1.53μm wavelength regime with optical pumping at the 1.48μm wavelength, counter-directionally.

Chapter II consists of brief theoretical reviews. Chapter III provides the details of device fabrication. Chapter IV presents optical testing method and experimental results. Finally, the summarized results are concluded in Chapter V.

CHAPTER II

THEORETICAL REVIEW

In this chapter propagation properties of optical waves in dielectric waveguides and anisotropic crystals are reviewed on the basis of Maxwell's equations. For the active rare earth element Er, the energy diagram is illustrated to show the optical absorption and radiation processes. Erbium incorporation into $LiNbO_3$ by in-diffusion is presented with the Fick's law and Arrhenius relation using measured SIMS (secondary ion mass spectroscopy) results.

A. Basic Theory of Wave Propagation

The fundamentals of the electromagnetic theory of waveguide propagation for isotropic, source-free, homogeneous, lossless dielectric, position- and time-dependent fields are governed by Maxwell's equations [9]

$$\nabla \times \mathbf{E} = -\frac{\partial \mathbf{B}}{\partial t} \tag{1}$$

$$\nabla \times \mathbf{H} = \frac{\partial \mathbf{D}}{\partial t} \tag{2}$$

$$\nabla \cdot \mathbf{D} = \mathbf{0} \tag{3}$$

$$\nabla \cdot \mathbf{B} = \mathbf{0} \tag{4}$$

where t is time, $\nabla = (\partial/\partial x, \partial/\partial y, \partial/\partial z)$ is the del operator, and **E** (V/m), **H** (A/m) are the

electric and magnetic field intensity vectors, and **D** (C/m^2), **B** (Wb/m^2) are the electric displacement and the magnetic displacement vectors. Medium properties determine the relations between **E** and **D** and between **B** and **H**. These relations are called as *constitutive relations*, expressed as [10]

$$\mathbf{D} = \varepsilon_0 \mathbf{E} + \mathbf{P} \tag{5}$$

$$\mathbf{B} = \mu_0 \mathbf{H} + \mu_0 \mathbf{M} \tag{6}$$

where **P** (C/m^2) and **M** (A/m) are the electric and magnetic polarization vectors of the medium, $\varepsilon_0 (= 8.85 \times 10^{-12}\ \mathrm{F/m})$ is the permittivity of free space, and $\mu_0 (= 4\pi \times 10^{-7}\ \mathrm{H/m})$ is the permeability of free space. When the dielectric properties of the medium are linear and isotropic, the polarizations are directly proportional to the intensity fields, and the proportionality constants are independent of the direction of the field. The polarization vectors are expressed as

$$\mathbf{P} = \varepsilon_0 (\varepsilon_r - 1)\mathbf{E} \tag{7}$$

$$\mathbf{M} = (\mu_r - 1)\mathbf{H} \tag{8}$$

where ε_r and μ_r are the relative permittivity and the relative permeability, and they characterize the effects of the atomic and molecular dipoles in the material and the magnetic dipole moments of the atoms constituting the medium [11].

By substituting the equations (7), (8) into (5), (6), the displacement vectors can be expressed in terms of two scalar quantities as

$$\mathbf{D} = \varepsilon\mathbf{E} = \varepsilon_0\varepsilon_r\mathbf{E} \tag{9}$$

$$\mathbf{B} = \mu\mathbf{H} = \mu_0\mu_r\mathbf{H} \tag{10}$$

The solution of Maxwell's equations in a source free isotropic medium can be obtained by taking the curl of equation (1), using equation (2), applying equations (3), (4), (9) and (10), and using the vector identity $\mathbf{A}\times\mathbf{B}\times\mathbf{C} = \mathbf{B}(\mathbf{A}\cdot\mathbf{C}) - \mathbf{C}(\mathbf{A}\cdot\mathbf{B})$, yielding

$$\nabla^2\mathbf{E} - \varepsilon\mu\frac{\partial^2\mathbf{E}}{\partial t^2} = 0. \tag{11}$$

For a monochromatic wave with angular frequency, $\omega = \frac{2\pi c}{\lambda}$, the electric field vector $\mathbf{E}$ can be expressed in a complex exponential form as

$$\mathbf{E}(\mathbf{r}, t) = \mathbf{E}(\mathbf{r})e^{j\omega t}. \tag{12}$$

Substituting equation (12) into equation (11), gives the well known *wave equation*, expressed as

$$\nabla^2\mathbf{E}(\mathbf{r}) + n^2k_0^2\mathbf{E}(\mathbf{r}) = 0 \tag{13}$$

where $k_0 = \frac{\omega}{c}$ is the propagation constant in free space, $c = \frac{1}{\sqrt{\mu_0\varepsilon_0}}$ is the speed of light in free space, and $n = \sqrt{\varepsilon_r}$ is the refractive index of the medium, with $\mu_r = 1$ for dielectric medium.

B. Optical Waveguide

A general optical waveguide has a physical structure to guide electromagnetic waves. Rectangular waveguides, the most useful waveguide configuration, consist of a rectangular core surrounded by a cladding with lower refractive index than that of the core [12]. The three dimensional rectangular waveguides is usually investigated for its transmission characteristics. However, numerical methods are needed to obtain exact solutions. A good insight for the solutions can be attained using a two dimensional waveguides structure, as depicted in Fig. 1.

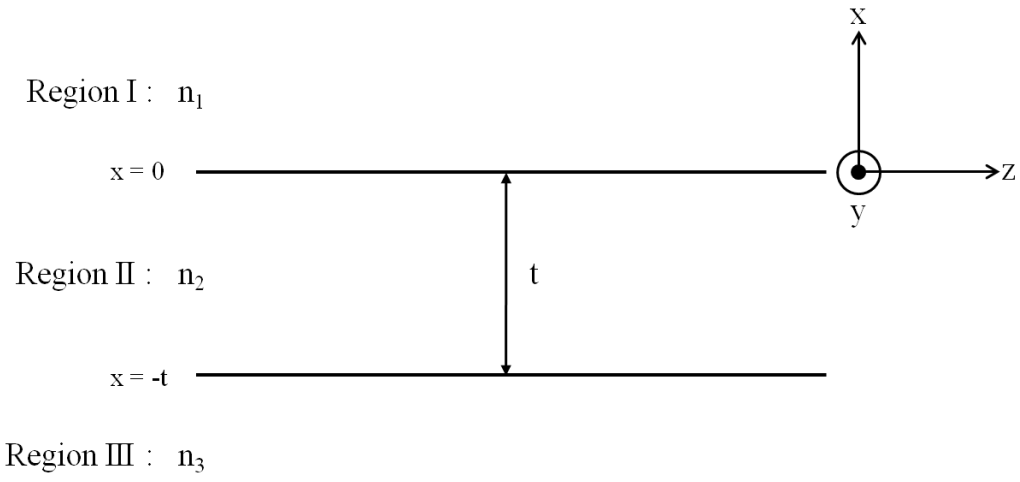

Fig. 1. Planar dielectric waveguide structure

The wave is assumed to have a forward z-propagation wave with propagation constant β, and electromagnetic field **E** and **H** do not have dependency along y-axis direction. And also, it is essential to have continuity of the tangential components for the electric field **E** and magnetic field **H**, and the normal components of the electric flux density **D** and magnetic flux density **B**, at the boundaries of different media.

To characterize the light transmission, it is necessary to understand modes propagation phenomena in the waveguide. For the light to propagate inside of the waveguide, it is essential to have index distribution of $n_2 > n_3 > n_1$ in the structure.

From the driven equation (13), the solution of the wave equation can define modes at a fixed frequency in a waveguide. For light propagation along z-axis, by redefining of equation (12) for electric field, it is expressed as

$$\mathbf{E}(\boldsymbol{r}) = \mathbf{E}(x, y, z) = \mathbf{E}(x, y)e^{-j\beta z}, \tag{14}$$

and also using the relation of the curl $\nabla^2 = \frac{\partial^2}{\partial x^2} + \cancel{\frac{\partial^2}{\partial y^2}} + \frac{\partial^2}{\partial z^2}$ due to no dependence on y-axis direction, equation (13) becomes [12]:

$$\text{Region I}: \ \frac{d^2}{dx^2}\mathrm{E}(x) + (k_0^2 n_1^2 - \beta^2)\mathrm{E}(x) = 0$$

$$\text{Region II}: \ \frac{d^2}{dx^2}\mathrm{E}(x) + (k_0^2 n_2^2 - \beta^2)\mathrm{E}(x) = 0 \tag{15}$$

$$\text{Region III}: \ \frac{d^2}{dx^2}\mathrm{E}(x) + (k_0^2 n_3^2 - \beta^2)\mathrm{E}(x) = 0$$

where E(x) is a Cartesian component of **E**(x) in each region.

Each region can be classified by the solution of equation (15) according to the value of $k_0 n_i$ (i = 1,2,3) relative to the propagation constant β. In a case where $\beta < k_0 n_1$, equation (15) requires to have sinusoidal solution in all three regions, which gives oscillatory or radiation modes in x-axis. This is the case that the light cannot be guided in region II. In another case where $k_0 n_1 < \beta < k_0 n_3$, it has sinusoidal behavior in region II and III, however it shows exponential decay in region I. This is the case called substrate radiation mode. In another case, where $k_0 n_3 < \beta < k_0 n_2$, it has only sinusoidal behavior in

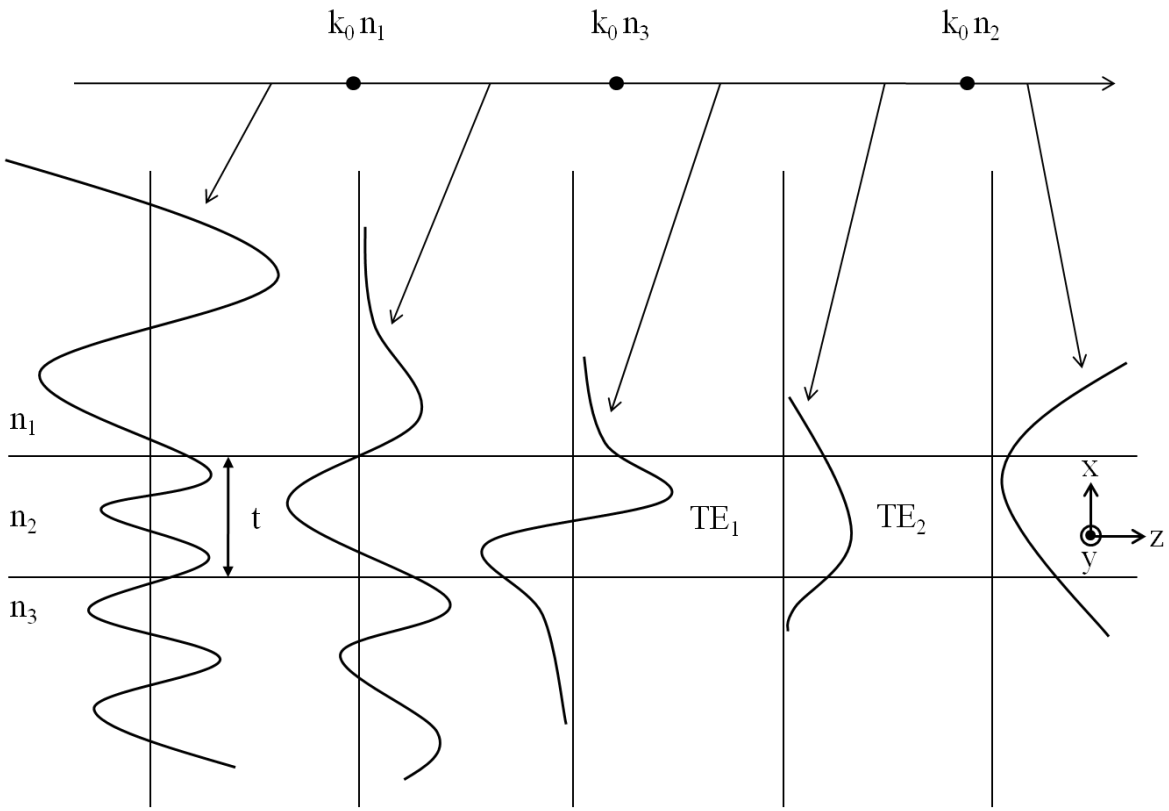

Fig. 2. The electric field distribution of the planar waveguide corresponding to different propagation constant β in a waveguide structure with $n_2 > n_3 > n_1$.

region II, however it also has exponential decay in region I and III. This provides only solutions for the existence of guided modes in the waveguide. In the other case where $\beta > k_0 n_2$, the solution of the electric field has an exponential increase in all three regions. This solution is a nonrealistic for energy conservation and is ignored. Fig. 2 illustrates the electric field distributions for the various described cases.

As a result, for guided modes propagation it is required that the condition $k_0 n_3 < \beta < k_0 n_2$ must be satisfied. In other words, the core region should have the highest refractive index relative to its surrounding regions.

The planar waveguide shown in Fig. 1 can support a finite number of guided modes. Those modes can be classified into two possible groups, with mutually orthogonal polarization states. One has that an electric field component along z-axis as zero since the electric field lies in the plane that is perpendicular to the z-axis [12].

This electromagnetic field distribution is called Transverse Electric (TE) mode. It consists of the field components of E_y, H_x, and H_z, and satisfies the following wave equations:

$$\frac{\partial^2 E_y}{\partial x^2} + (k_0^2 n^2 - \beta^2) E_y = 0 \tag{16}$$

where

$$\mathbf{E}(\mathbf{r}, t) = E_y(x) e^{i(\omega t - \beta z)}.$$

The magnetic field components can then be obtained from

$$\mathrm{H}_x = -\frac{\beta}{\omega\mu_0}\,\mathrm{E}_y$$

$$\mathrm{H}_z = -\frac{1}{j\omega\mu_0}\frac{\partial \mathrm{E}_y}{\partial x}$$

Using equation (16) and the condition for guided modes propagation, the electric field distribution at each region can be expressed as

$$\mathrm{E}_y(x) = \begin{cases} Ce^{-qx} & \text{, at Region I} \\ C\left[\cos(hx) + \frac{q}{h}\sin(hx)\right] & \text{, at Region II} \\ C\left[\cos(ht) + \frac{q}{h}\sin(ht)\right]e^{p(x+t)} & \text{, at Region III} \end{cases} \tag{17}$$

where $h = \sqrt{k_0^2 n_2^2 - \beta^2}$, $p = \sqrt{\beta^2 - k_0^2 n_3^2}$, $q = \sqrt{\beta^2 - k_0^2 n_1^2}$, C is an arbitrary constant, and t is the thickness of the planar waveguide. The electric and magnetic field components, E_y, H_z, should be continuous at the boundaries of x=0 and x=-t. From the preceding relations, eigenvalue equation, or characteristic equation for TE mode can be obtained as

$$\tan(ht) = \frac{p+q}{(h - \frac{q}{h}p)} \tag{18}$$

when the indices, n_1, n_2, and n_3, of the waveguide materials, the guide thickness, *t*, and wavelength, λ, are known, a value of *h* can be obtained from the equation (18). However, the value could be more than one depending on the indices, thickness and wavelength. Each *h* value corresponds to a mode.

The other has that the magnetic field component along the z-axis as zero since the magnetic field lies in the plane that is perpendicular to the z-axis [12]. This electromagnetic field distribution is called Transverse Magnetic (TM) mode. It consists of the field components of E_x, H_y, and E_z, and satisfies the following wave equations:

$$\frac{\partial^2 H_y}{\partial x^2} + (k_0^2 n^2 - \beta^2) H_y = 0 \tag{19}$$

where

$$\mathbf{H}(\mathbf{r}, t) = H_y(x) e^{i(\omega t - \beta z)}$$

$$E_x = \frac{\beta}{\omega \varepsilon_0 n^2} H_y$$

$$E_z = \frac{1}{j\omega \varepsilon_0 n^2} \frac{\partial H_y}{\partial x}$$

The finite number of eigenvalues identifies the number of modes inside a waveguide. Each mode is associated with a specific effective index value. The lowest order mode is the fundamental mode. To avoid dispersion in practical applications, waveguides are designed to support only the fundamental mode, as a single mode.

C. Optical Indicatrix in Uniaxial Crystals

In an isotropic medium the electric and polarization field vectors of **E** and **P** are parallel to each other and linearly related through a scalar electric susceptibility χ_e. In contrast, **E** and **P** are not necessarily parallel in an anisotropic medium, due to the susceptibility dependence on direction, and the relation is expressed as

$$\mathbf{P} = \varepsilon_0 \tilde{\chi}_e \mathbf{E} \tag{20}$$

where $\tilde{\chi}_e$ denotes a 3 x 3 tensor. The electric displacement vector **D** and the electric intensity **E** vector are consequently related by means of the dielectric permittivity tensor $\tilde{\varepsilon}$

$$\mathbf{D} = \tilde{\varepsilon}\mathbf{E} \tag{21}$$

where $\tilde{\varepsilon} = \varepsilon_0(\mathrm{I} + \tilde{\chi}_e) = \varepsilon_0 \tilde{\varepsilon}_r$. The dielectric tensor elements depend on the crystalline material symmetry. The simplest form of anisotropy appears in uniaxial crystals, such as $LiNbO_3$, and exhibit symmetry about a single axis, called the optic axis, with $n_x = n_y \neq n_z$. In a diagonalized system, the permittivity can be written as [9]

$$\tilde{\varepsilon} = \begin{bmatrix} \varepsilon_{11} & 0 & 0 \\ 0 & \varepsilon_{22} & 0 \\ 0 & 0 & \varepsilon_{33} \end{bmatrix} \tag{22}$$

where $\varepsilon_{11}, \varepsilon_{22}, \varepsilon_{33}$ are defined as principal permittivities. Using the relation $\varepsilon = \varepsilon_0 \varepsilon_r = \varepsilon_0 n^2$, the matrix (22) can be rewritten as

$$\tilde{\varepsilon} = \varepsilon_0 \begin{bmatrix} n_x^2 & 0 & 0 \\ 0 & n_y^2 & 0 \\ 0 & 0 & n_z^2 \end{bmatrix} \tag{23}$$

where n_x^2, n_y^2, n_z^2 represent refractive indices along the principal axes. Extending the defining relation of the electric energy density U_e in an anisotropic medium,

$$U_e = \frac{1}{2}\mathbf{E} \cdot \mathbf{D} \tag{24}$$

to a diagonalized anisotropic material, leads to

$$\begin{aligned} U_e &= \frac{1}{2}\left[\varepsilon_{11}\mathrm{E}_x^2 + \varepsilon_{22}\mathrm{E}_y^2 + \varepsilon_{33}\mathrm{E}_z^2\right] \\ &= \frac{1}{2}\left[\frac{\mathrm{D}_x^2}{\varepsilon_{11}} + \frac{\mathrm{D}_y^2}{\varepsilon_{22}} + \frac{\mathrm{D}_z^2}{\varepsilon_{33}}\right] \end{aligned} \tag{25}$$

Defining unit quantities *x*, *y*, *z* along the crystal 3-pricipal axes as $x = \frac{D_x}{\sqrt{2\varepsilon_0 U_e}}, y = \frac{D_y}{\sqrt{2\varepsilon_0 U_e}}, z = \frac{D_z}{\sqrt{2\varepsilon_0 U_e}}$, reduces equation (25) to [9]

$$\frac{x^2}{n_x^2} + \frac{y^2}{n_y^2} + \frac{z^2}{n_z^2} = 1, \tag{26}$$

with $n_x^2 = \frac{\varepsilon_{11}}{\varepsilon_0}, n_y^2 = \frac{\varepsilon_{22}}{\varepsilon_2}$ *and* $n_z^2 = \frac{\varepsilon_{33}}{\varepsilon_0}$. Equation (25) represents an index ellipsoid, or indicatrix. It has semi-axes of the ellipsoid $\left(n_x = \sqrt{\frac{\varepsilon_{11}}{\varepsilon_0}},\ n_y = \sqrt{\frac{\varepsilon_1}{\varepsilon_0}},\ n_z = \sqrt{\frac{\varepsilon_{11}}{\varepsilon_0}}\right)$. In uniaxial crystals, $n_x = n_y \equiv n_o$ and $n_z \equiv n_e$ as

$$\frac{x^2}{n_o^2} + \frac{y^2}{n_o^2} + \frac{z^2}{n_e^2} = 1 \tag{27}$$

where n_o and n_e represent ordinary and extra-ordinary indexes of refraction. The index ellipsoid for uniaxial crystals is shown in Fig. 3, and exhibits symmetry about the z-axis. The index ellipsoid provides a means for identifying allowed polarization directions for a given direction of propagation ***k***, and ultimately their corresponding refractive indices.

The allowed polarization directions and indices of refraction for a given direction of propagation ***k*** can be found from the intersection of a plane through the origin that is normal to ***k*** with the index ellipsoid. As shown in Fig. 3, the intersection produces the shaded ellipse. The directions of the major and minor axes of the ellipse define the directions of the two allowed polarizations for the electric displacement vectors ***D***. One is $\boldsymbol{D_e}$ which is parallel to the major axis OA of the ellipse, and it is called the extraordinary polarized wave with an index of refraction $n_e(\theta)$.

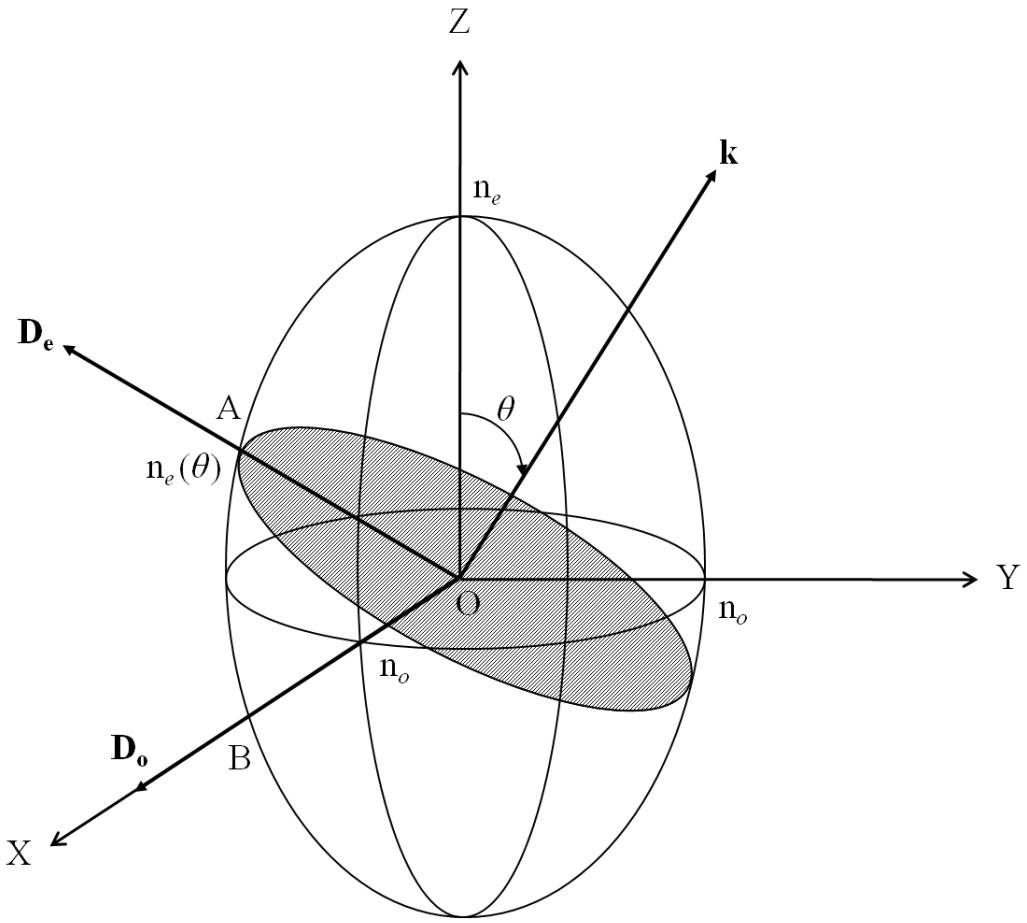

Fig. 3. Optical indicatrix (index ellipsoid) for a uniaxial crystal

The other is $\boldsymbol{D_o}$ which is parallel to the minor axis OB, and it is called the ordinary polarized wave with a constant index of refraction n_o.

$$\frac{1}{n_e^2(\theta)} = \frac{cos^2\,\theta}{n_o^2} + \frac{sin^2\,\theta}{n_e^2} \tag{28}$$

The refractive index of an extraordinary wave varies from $n_e(\theta) = n_o$ for $\theta = 0^\circ$ to $n_e(\theta) = n_e$ for $\theta = 90^\circ$. For $\theta = 0^\circ$, the crystal behaves like an isotropic material which has cubic symmetry.

D. Erbium Energy Level System

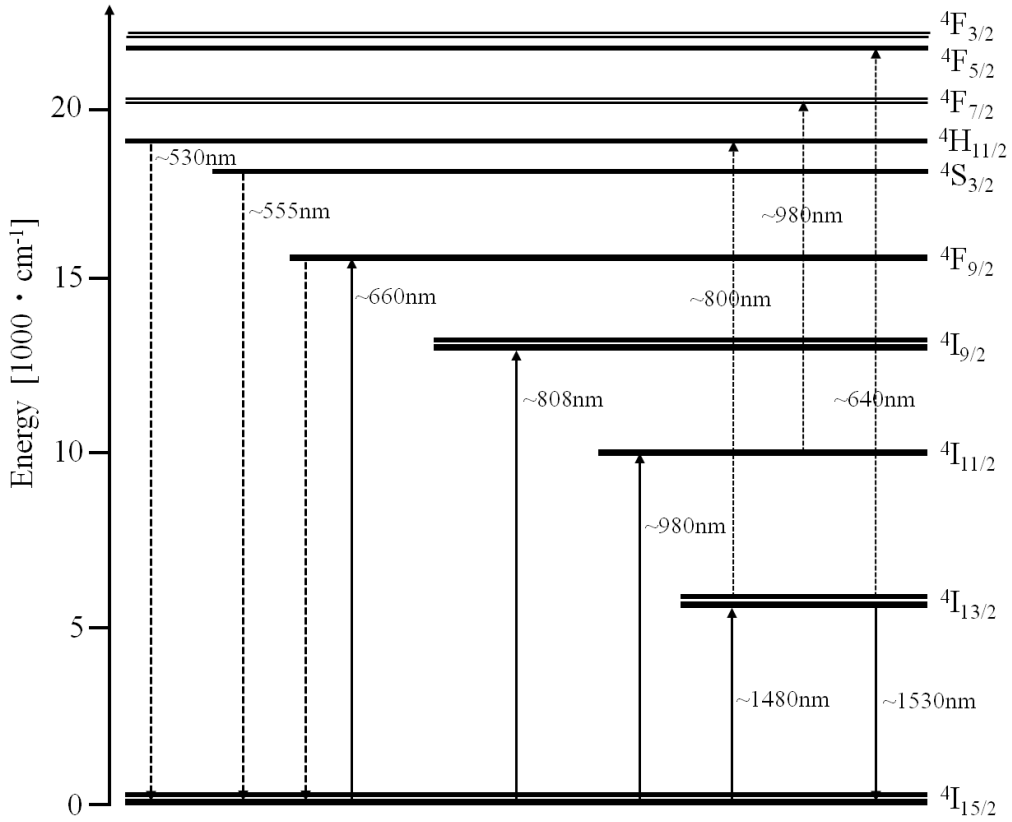

Fig. 4. Energy level scheme of Er^{3+} in $LiNbO_3$

Fig. 4 illustrates the energy levels distribution of Er in $LiNbO_3$. The upward pointing arrows represent possible transitions by optical pumping to populate high

energy levels. The downward pointing arrows represent radiative or nonradiative transition from the upper level to the ground state. According to the ratio of the population densities of level $^4I_{13/2}$ and level $^4I_{15/2}$, the transitions correspond to absorption at 1480nm wavelength and radiation emission in the wavelength range from 1440nm to 1640nm [13].

Significant absorption is also observed in the visible (530nm < λ < 660nm) and near-infrared (808nm < λ < 980nm) wavelength range. These absorptions lead to excited states, and are indicated with the upward pointing dotted-lines in Fig. 4. The preferred absorption band for stimulated emission near 1530nm is by optical pumping at λ_P=1480nm. There are possible decay channels to the ground state, which diminish optical gain by reducing the population density of the $^4I_{13/2}$ level [13]. The decay channels lead to ground state absorption (GSA) via transitions from the ground state level $^4I_{15/2}$ to levels $^4F_{9/2}$, $^4S_{3/2}$, $^4H_{11/2}$ followed by a fast relaxation via radiative and nonradiative transitions into the level $^4I_{13/2}$ [14]. However the decay channels are very weak when 1480nm optical pumping is used. Furthermore, single mode waveguides can be readily fabricated in $LiNbO_3$ to support both signal and pump beams [14].

E. Erbium Diffusion

As an Er-doping method, diffusion of a vacuum-deposited Er-film is the simplest and most efficient technique yielding high-quality striation-free crystals of high doping concentration [15]. The diffusion constants and the solubility of erbium are important factors for the fabrication of low-loss Er-doped Ti diffused waveguide amplifier with

optimized overlaps between evolving gain cross section and intensity distribution of the guided mode [15]. To determine the diffusion influence, a careful examination of the concentration profiles of Er and Ti is necessary.

The diffusion profile of erbium into $LiNbO_3$ is well approximated by the one dimensional diffusion equation, described by Fick's law

$$\frac{\partial C}{\partial t} = D\frac{\partial^2 C}{\partial y^2} \tag{29}$$

where y is the direction normal to the substrate surface, and *D* is the diffusion coefficient. The solution of equation (29) from a thick Er film as the source is a complementary error function:

$$C(y) = C_0\, erfc\left(\frac{y}{d}\right), \tag{30}$$

where C_0 is the erbium concentration at the substrate surface and *d* is the diffusion depth, $2\sqrt{Dt}$. If the diffusion is from a thin Er film, the source is depleted rapidly and the diffusion profile can be approximated by the Gaussian function:

$$C(y) = \tilde{C}_0 exp\left(\frac{-y^2}{4Dt}\right), \tag{31}$$

with the erbium surface concentration corresponding to the maximum solubility:

$$\tilde{C}_0 = \frac{\tau C_0}{\sqrt{\pi D t}} \leq C_0$$

where τ is the initial thickness of the erbium film.

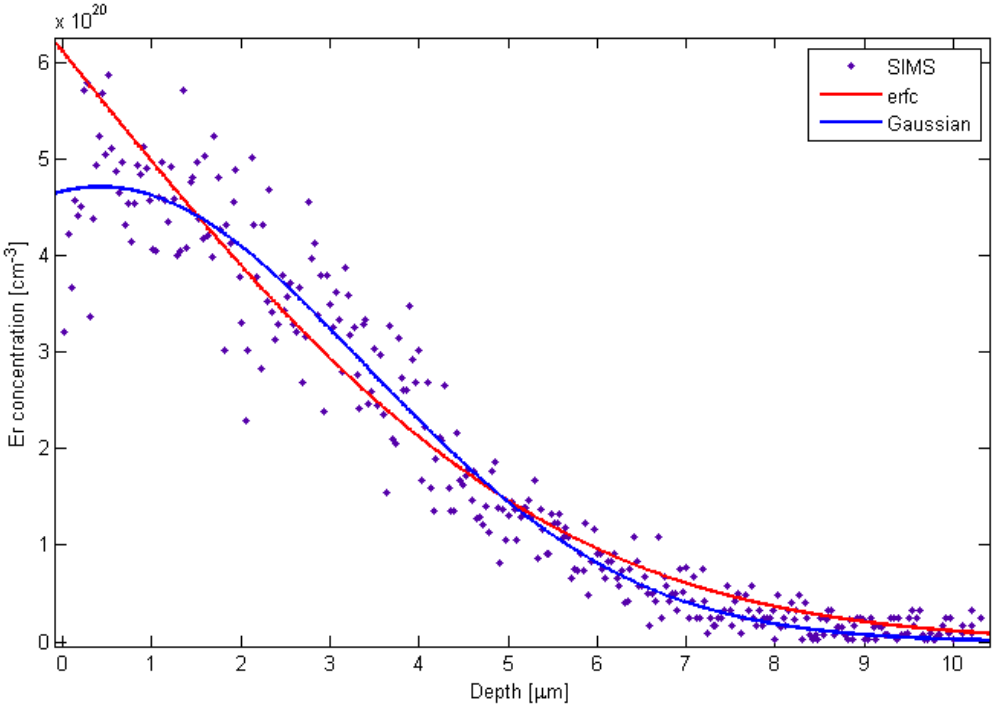

Fig. 5. SIMS erbium depth profile of 9nm-thick Er diffusion for 96 hours into x-cut $LiNbO_3$ at 1100˚C.

The diffusion coefficient D and surface concentration C_0 can be obtained from the erbium concentration profile in Fig. 5., which shows the least square fit of

complementary error function (red-solid line), corresponding to equation (31) and the Gaussian function (blue-solid line), corresponding to the equation (32). The fits are made to measured SIMS data points obtained from an Er doped $LiNbO_3$ sample produced by diffusing 9nm-thick Er film at 1100˚C for 96 hours.

The diffusion coefficient D can be obtained from the Arrhenius relation of diffusion constant D_0 and the activation energy E_a for diffusion, which is given by

$$D = D_0 exp\left(-\frac{E_a}{k_B T}\right) \tag{32}$$

where k_B is Boltzmann's constant and T is the diffusion temperature in Kelvin.

Using the equation (30), (31) and (32) with the SIMS erbium depth profile data, the diffusion coefficient D is found to be $2.29 \times 10^{-13}\text{cm}^2/\text{s}$. The obtained diffusion coefficient D is comparable to the measured values $(1.33 \times 10^{-13}\text{cm}^2/\text{s})$ reported by Baumann *et al.* [15] and $(0.71 \times 10^{-13}\text{cm}^2/\text{s})$ Caccavale *et al.* [16]. Table 1 is for the diffusion constants and activation energy for erbium diffusion in x-cut $LiNbO_3$.

Table 1. Diffusion constants and activation energy for erbium diffusion in x-cut $LiNbO_3$ [15]

D_0 [$\times 10^{-5}\text{cm}^2/\text{s}$]	E_a [eV]
12.0 ± 2.0	2.44 ± 0.04

CHAPTER III

DEVICE FABRICATION

Devices were fabricated using the following as control parameters: erbium thickness, erbium doping dimension, erbium in-diffusion duration, titanium thickness, titanium in-diffusion duration, and diffusion temperature. A step-by-step outline of the fabrication procedure is described in Appendix 1, and details of each process of the fabrication are listed in subsequent appendixes.

A. $Ti:LiNbO_3$ Waveguide and $Ti:Er:LiNbO_3$ Waveguide Amplifier

The fabrication of erbium doped titanium diffused waveguide amplifier starts with preparation of appropriate size of substrates by dicing 1mm thick, 3" diameter x-cut y-propagating $LiNbO_3$ crystal wafers supplied by Crystal Technology Inc. (Palo Alto, CA) into the size of 41mm-long (y-axis) × 16mm-wide (z-axis) substrate samples (Appendix 2). The diced substrates were thoroughly cleaned with liquid solvents (Appendix 3). Cleaning the sample is very important to make sure that it is free from any dust, dirt, or residual particles. A negative photolithography process (Appendix 4) was used to delineate a specific dimension of photoresist patterns for the selective erbium doping on the cleaned sample. The sample was dehydrated for 5 minutes at 135˚C in the oven, and spin-coated with Clariant AZ-5214E photoresist. Dehydration is a critical step to evaporate any H_2O residue from the sample, and to prevent the photoresist pattern from adhering to the H_2O residue. Pre-baking was done for 2 minutes at 120˚C on a hot

plate. Then the sample was exposed to UV light using Karl Suss mask aligner, MJB3, by aligning with a $4.0" \times 4.0" \times 0.06"$ quartz mask plate containing the desired patterns (Appendix 5). After the exposure to UV light power density of 8.3mW/cm^2 for 1 minute, post-baking was carried out for 1 minute at 120˚C on a hot plate. This is a critical step in the image reversal process to promote crosslinking of the polymer resin in the exposed areas of photoresist. The crosslinked photoresist becomes insoluble in the developer solution. Flood exposure was carried out without the patterned quartz mask with the UV light power density of 8.3mW/cm^2 for 1 minute. After the flood exposure process, the sample was developed in Shipley MF319 developer so that all the photoresist remains on the sample except the patterned region. Next, the sample was further cleaned with oxygen plasma (Appendix 6) for 3 minutes, and vacuum hard baked at 135˚C for 15 minutes. The purpose of oxygen plasma is to remove unwanted photoresist residue from the image reversed pattern, and the vacuum hard baking is for hardening the patterned photoresist.

A thin film of erbium (Er) was deposited on the patterned sample's surface using DC magnetron-sputtering process (Appendix 7). To have erbium deposited region only over the image reversed pattern out of the entirely erbium deposited surface on the sample, lift-off process was accomplished with Acetone in a sonicator for 1 hour. Then the sample was cleaned with liquid solvents, and the erbium patterned film thickness was measured by atomic force microscopy (AFM) and Dektak^3 Surface Profile Measuring System. The reason to have two measuring method is that the Dektak^3 has a minimum resolution feature which is very close to deposited Er thickness, so to check

out the right thickness, AFM, which has a much lower minimum resolution feature, was used. After thoroughly cleaning the sample with liquid solvents, diffusion process was carried out in a 48mm x 35mm x 10mm of platinum (Pt) box to prevent LiO_2 out-diffusion from the $LiNbO_3$ surface, which can cause the $LiNbO_3$ surface damage during the erbium diffusion. The Pt box containing the sample was placed into a quartz tube furnace and the Er film diffused into the substrate at a certain temperature and duration (Appendix 8).

There are two relevant factors in a diffusion process: diffusion temperature and diffusion duration. The diffusion temperature is a more critical one as indicated by the following diffusion depth equation [15]:

$$d = 2 \times \sqrt{D_{Er} t} \tag{33}$$

where D_{Er} is the Er diffusion coefficient given by equation (32) in Chapter II and t is the diffusion duration. Using the obtained erbium diffusion coefficient ($D_{Er} = 2.29 \times 10^{-13} cm^2/s$) and the used experimental erbium diffusion time (t = 100 hours), the calculated diffusion depth is 5.75μm. Fig. 6 shows the erbium diffusion depth as a function of time t using equation (33) with the obtained diffusion coefficient.

The diffusion was carried out in argon (Ar) ambient while oxygen (O_2) was used during the initial warm-up to 1100°C and final cool off to room temperature. The reason the diffusion was performed in a dry oxygen atmosphere during the initial warm-up was to fully oxidize the erbium layer followed by diffusion in argon atmosphere. The last

hour of diffusion was carried out in oxygen atmosphere to compensate for any losses from oxygen of the crystal during the diffusion [15]. Erbium diffused $LiNbO_3$ substrate was visually inspected under a microscope to ensure the absence of defects on the $LiNbO_3$ surface.

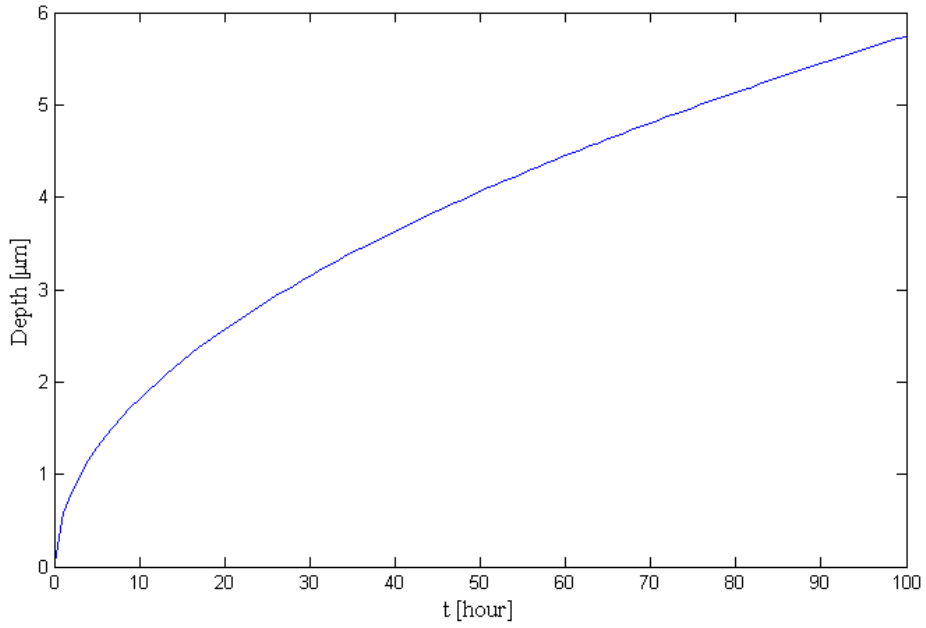

Fig. 6. Er diffusion depth as a function of time *t* using the diffusion depth equation with $D = 2.29 \times 10^{-13} cm^2/s$ and t = 100 hours

The selectively erbium doped $LiNbO_3$ substrate was then thoroughly cleaned with liquid solvents. A thin film of titanium was deposited over the entire substrate surface using DC sputtering process (Appendix 9). A positive photolithography process (Appendix 10) was used to delineate 7µm-wide straight channel waveguide patterns

upon both the erbium doped and undoped regions. The substrate was dehydrated for 5 minutes at 135˚C in the oven, and spin-coated with Clariant AZ-5214E photoresist. Soft-baking was done for 2 minutes at 120˚C on a hot plate. This process was required to increase adhesion between the titanium film and the photoresist. Then the substrate was exposed to UV light using Karl Suss mask aligner, MJB3, by aligning with a 4.0" × 4.0" × 0.06" quartz mask plate containing the desired patterns (Appendix 11). After exposure to UV light power density of 11mW/cm^2 for 4.7 seconds, it was developed in Shipley MF319 developer so that photoresist remained only at the straight waveguide patterns. The photoresist patterns were visually inspected under a microscope to ensure the quality of the waveguide patterns. The patterned sample was hard-baked at 135˚C for 15 minutes in an oven to harden the photoresist. This process was necessary to help the patterns endure reactive ion etching (RIE) process (Appendix 12) for dry etch and for the following diluted HF acid wet etch. To avoid surface damage on the $LiNbO_3$ substrate during reactive ion bombardment, a thin residual titanium layer was left on the sample. The remaining titanium layer was removed by using diluted HF acid (HF: DI water, 1:10). The sample was then immersed into the photoresist stripper solution (Clariant, AZ 300T) and heated up to 90˚C to remove all photoresist from the delineated waveguide patterns of the sample surface. The Ti patterns on the sample were visually inspected under a microscope to ensure the line width uniformity. Then titanium pattern thickness was measured by Dektak^3 Surface Profile Measuring System. Prior to the diffusion process, the sample was well cleaned in liquid solvents.

After the thorough cleaning titanium in diffusion process was carried out in wet

breathing air ambient to reduce the out-diffusion of LiO_2 from the $LiNbO_3$ surface, which could cause unwanted planar guiding for the extraordinary polarization (TE), which would be along the z-axis of the crystal. The water vapor suppresses the out-diffusion. Since the strongest electro-optic coefficient for $LiNbO_3$, r_{33}, affects light of the extraordinary polarization, out-diffusion can be a significant problem in the fabrication of efficient optical waveguide device [17]. The sample sat on an alumina boat, and it was inserted into an alumina tube. Then the sample was placed into a quartz tube furnace at a certain temperature and duration (Appendix 13). After the diffusion the samples were visually inspected under a microscope.

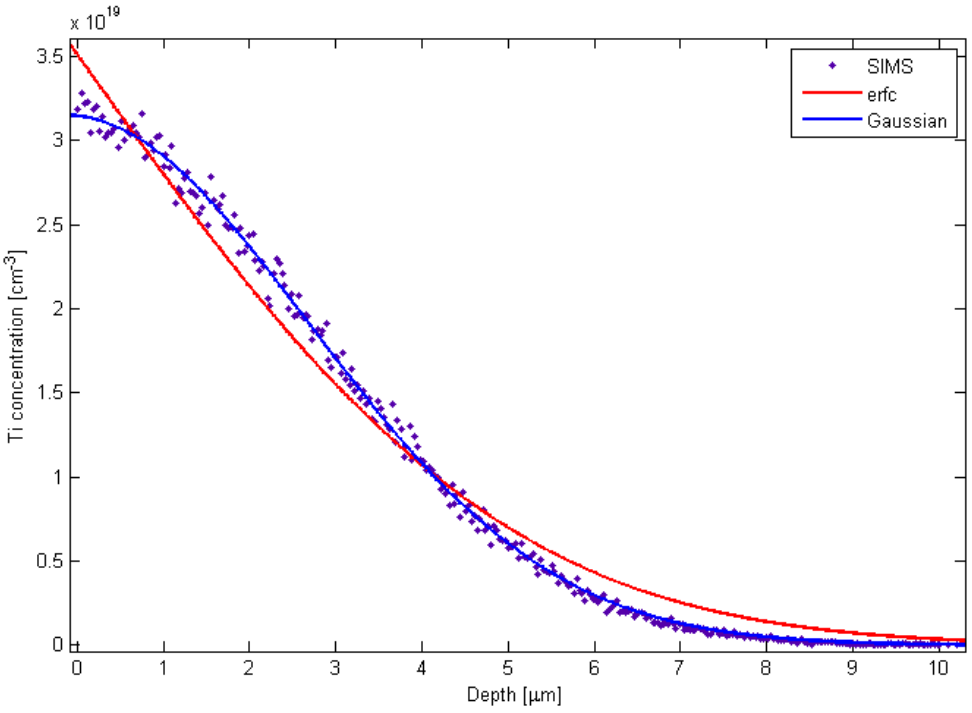

Fig. 7. SIMS titanium depth profile with erfc function fit and Gaussian function fit for 1100Å-thick Ti diffusion for 11 hours at 1025˚C into x-cut $LiNbO_3$.

The titanium diffusion coefficient D_{Ti} and surface concentration C_0 can be obtained from the titanium concentration profile in Fig. 7., which shows the least square fit of complementary error function (red-solid line), corresponding to equation (31) and the Gaussian function (blue-solid line), corresponding to equation (32). The fits are made into the measured SIMS data points.

Using the obtained titanium diffusion coefficient (D_{Ti} = 9.55 x 10^{-13}cm^2/s) and the experimental titanium diffusion time (t = 11 hours), the calculated titanium diffusion depth is 3.89μm. This depth value is comparable to the value obtained with commonly used diffusion coefficient equation:

$$D = D_0 \times exp\left(-\frac{T_0}{T}\right) \tag{34}$$

where D_0 is bulk diffusivity and T_0 is the activation temperature. Both values are dependent on the composition of lithium niobate substrate. Commonly used 48.6 mole % of Li_2O in $LiNbO_3$ has $D_0 = 2.5\times10^{-4}$ cm^2/s and $T_0 = 2.5 \times 10^4$ K. Using equation (34) with the listed reported values, it gives D = 1.08 x 10^{-13}cm^2/s, and the diffusion depth is 4.14μm, which is very close to the value from the SIMS analysis.

As a final step, for the optical testing, the sample was polished along both end side facets perpendicular to the waveguides (Appendix 14). A good optical finish and a 90˚ edge are required at both the input and output optical facets to ensure good fiber-to-waveguide coupling [18]. In order to eliminate reflections caused by coupling, the more

advanced industry practice is to polish the substrate end surface at an angle to the waveguides.

Fig. 8 is a schematic of the final device configuration. Another structure that was used at the initial stage of the research is illustrated in Fig. 9.

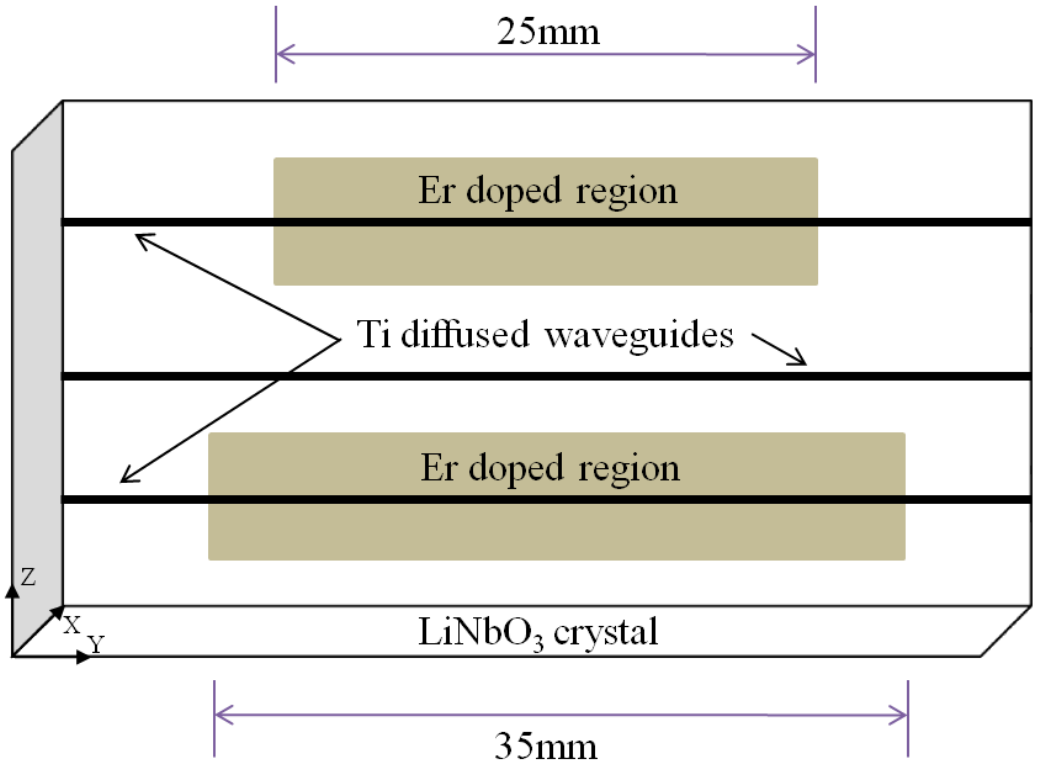

Fig. 8 Schematic diagram of Ti:$LiNbO_3$ and Ti:Er:$LiNbO_3$ waveguides

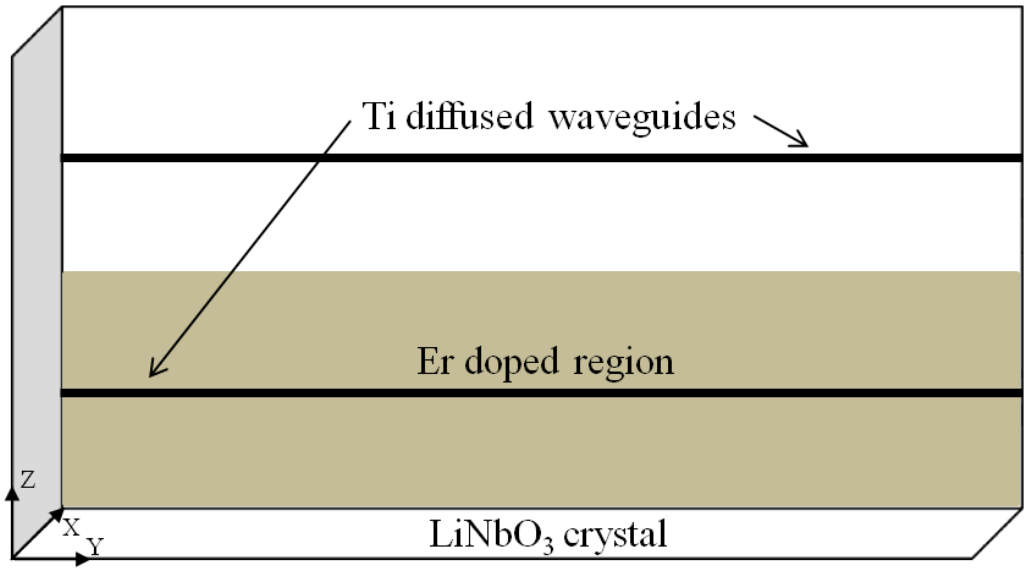

Fig. 9 Schematic diagram of Ti:$LiNbO_3$ and Ti:Er:$LiNbO_3$ waveguides

CHAPTER IV

OPTICAL TESTING AND EXPERIMENTAL RESULT

In this chapter, the experimental performance results of straight channel waveguide and selectively erbium doped channel waveguide amplifier are given. The characterization of the device with respect to insertion loss, mode size, absorption loss, signal enhancement, net gain, and pump power are presented. Suggestion to improve the performance of the device is proposed.

A. Ti Diffused Channel Waveguide and Er-doped Ti Diffused Waveguide

High quality channel waveguides are essential in integrated optics. A high quality channel waveguide refers to an optical waveguide with a single mode, low propagation loss, strong confinement of light and excellent near field intensity mode profile. The titanium diffused straight channel waveguides on $LiNbO_3$ were fabricated to have such qualities. The test setup shown in Fig. 10 was used for the loss characterization. Light is coupled in and out of the device with a single mode fiber. The propagation loss can be calculated from input and output power measurements, which is denoted the insertion loss and expressed as

$$\text{Insertion loss [dB]} = -10 \cdot \log \frac{P_{out}}{P_{in}} \tag{35}$$

where P_{in} and P_{out} are the measured output powers before and after placing the waveguide, respectively. The insertion loss includes coupling loss and propagation loss. The coupling loss consists of reflection (or Fresnel) loss at the two end interfaces of the substrate and the loss caused by mismatch between the fiber mode and waveguide modes [19]. Index matching liquid (IML) was used during measurements to reduce reflections and ensure maximum transmittance.

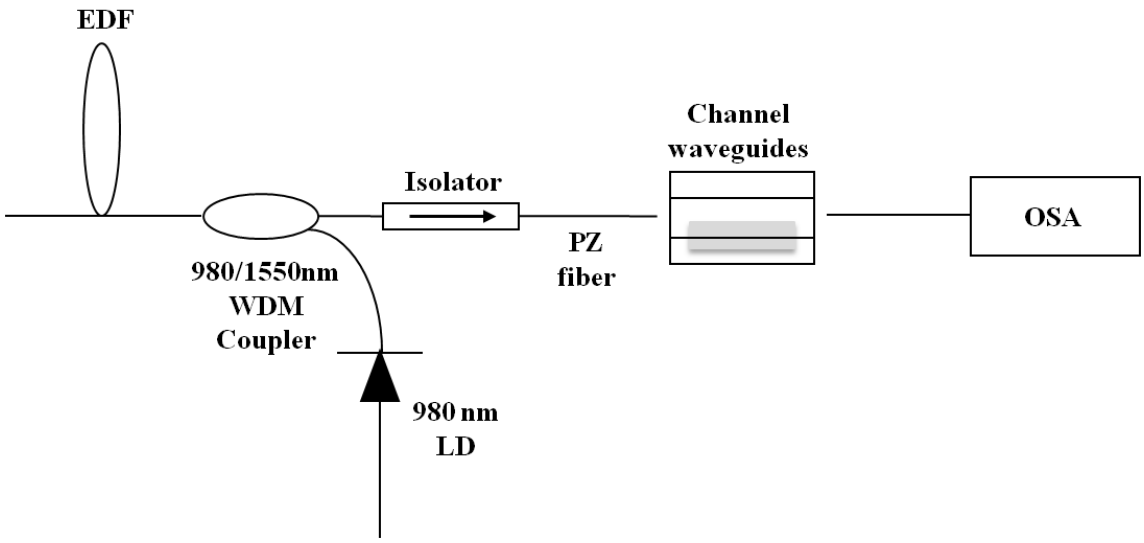

Fig. 10. Testing setup for insertion loss measurement of Ti:$LiNbO_3$ and Ti:Er:$LiNbO_3$ waveguides

A 10m long erbium doped fiber (EDF) was pumped by a 980nm laser diode (Lasertron, MA, Model QLM9S473-217) through a WDM coupler and Amplified Spontaneous Emission (ASE) light form the Erbium-doped Fiber Amplifier (EDFA) was used as a broadband light source for an incident input signal. An optical isolator was

included at the output of the coupler to prevent external cavity self-oscillation. The light was then guided though a polarizing fiber (PZ fiber) and rotated to have Transverse Magnetic (TM) polarization for the input signal that was launched into the waveguide. The emerging light from the output of the device was coupled into a single mode fiber (Corning SMF-28™). The output of the single mode fiber was displayed on an Optical Spectrum Analyzer (OSA, Anritsu, Model MS9710C). Fig. 11 shows the ASE output spectrum when the 980nm pump diode was driven at 25.2mA.

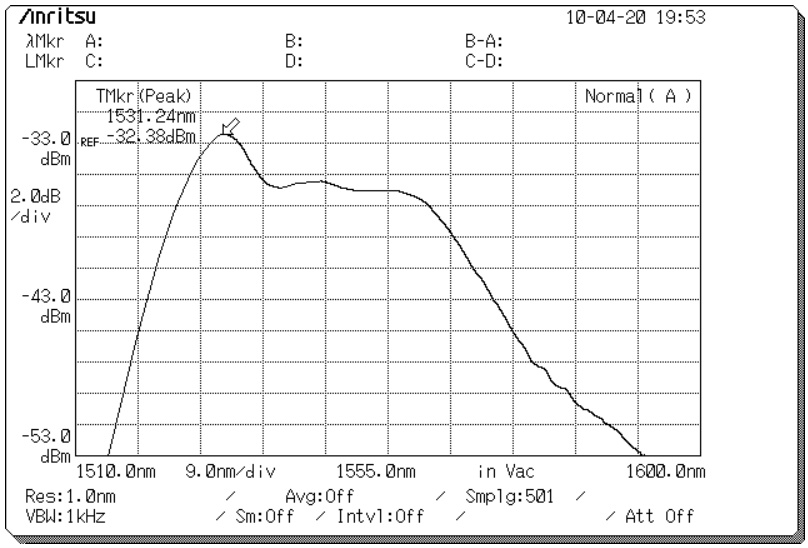

Fig. 11. Spectral output as a function of wavelength for the ASE output driven at pump current of 25.2mA

The insertion loss measurement values are listed in table 2 along with the fabrication parameters for 7μm-wide straight titanium in-diffused waveguide on sample ER21, which also included erbium doped region as shown in Fig. 8. All the samples

were fabricated with substrate dimensions of $41\text{mm} \times 16\text{mm} \times 1.0\text{mm}$. The length of the samples was re-measured after polishing the end facets. The final sample length was 39mm. The measured insertion losses of sample ER21 for TM polarization are 3.44dB for the Ti-diffused waveguide, 10.50dB for the 25mm-long Er-doped waveguide, and 12.26dB for the 35mm-long Er-doped waveguide. The Er-doped waveguides have much higher insertion loss than the one of the non-doped waveguide due to the Er.

Table 2. Insertion loss of Ti diffused waveguide, 25mm-long Er-doped Ti diffused waveguide and 35mm-long Er-doped Ti diffused waveguide of the total sample length of 39mm-long, using Index Matching Liquid (IML) at Transverse Magnetic (TM) mode.

	Sample: ER21		
	Ti-diffused waveguide	25mm-long Er-doped Ti:$LiNbO_3$	35mm-long Er-doped Ti:$LiNbO_3$
Er thickness [nm]	N/A	17	
Er diffusion time [Hour] / temperature [˚C]	N/A	100 / 1100	
Ti thickness [Å]	1070		
Ti diffusion time [Hour] / temperature [˚C]	10 / 1025		
Insertion loss [dB]	3.44	10.50	12.26

The propagation loss is needed for determining the gain of a Ti:Er:$LiNbO_3$ waveguide amplifier. The propagation loss can be obtained by subtracting the mode mismatch loss and reflection (Fresnel) loss from the measured insertion loss value. The mode mismatch contribution can be calculated from knowledge of the near field

intensity distributions for the waveguide mode and the fiber mode. Fig. 12 shows the test setup for obtaining the near field intensity mode profile of the waveguide. The same setup can also be used for obtaining the fiber mode profile by removing the sample and imaging the near field intensity from the output of the fiber.

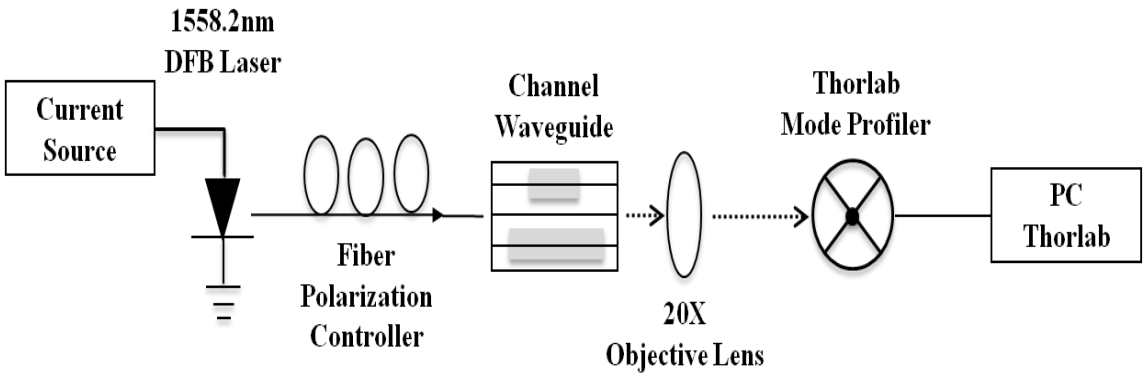

Fig. 12. The test setup for the field intensity mode profile measurement.

A pigtailed 1558.2nm distributed feedback (DFB) laser diode (Alcatel, Module: A 1915 LMI) controlled by a current source (ILX Lightwave, Model LDC-3712) at 36.8mA was used as an optical source to supply 1.0mW of optical power. The output of the laser diode was spliced to a single mode fiber (Corning SMF-28™) and the fiber was wounded into a fiber polarization controller (Thorlabs Inc., Model FDC010) to select the transverse magnetic (TM) mode for the input light. To ensure normal incidence of light on the end facet of the waveguide, the beam was coupled with a fiber holder mounted on a high resolution x-y-z translation stage (Line Tool Co., Allentown, PA). After propagating through the waveguide, the emerging beam was coupled through a 20X

objective lens and focused exactly at the image plane on the mode profiler (Thorlabs Inc., Model BP109-IR). Then, a computer installed with Thorlabs software (Thorlabs Mode Profiler) displays the near field intensity mode distribution of the beam in horizontal direction for a lateral mode profile and vertical direction for a depth mode profile, contour graphs of the intensity distribution, and also acquires data points of the mode profile.

Fig. 13 shows the obtained mode profiles of transverse lateral width and depth distributions for transverse magnetic (TM) polarization on a 7μm-wide Ti in-diffused waveguide in sample ER21. The continuous distribution with a single peak in the profiles, confirms that the waveguide supports only single mode propagation at the wavelength range near λ = 1.5μm.

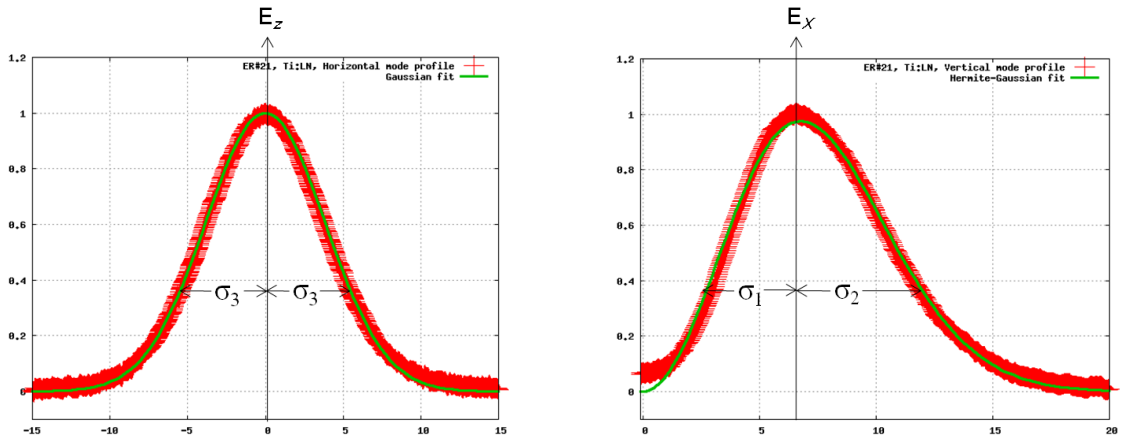

(a) Lateral mode profile of TM mode (b) Depth mode profile of TM mode

Fig. 13. Mode profiles of 7μm-wide Ti diffused channel waveguide in sample ER21 with (a) Gaussian function fit and (b) Hermite-Gaussian function fit

The data plot was taken and fitted into Gaussian distribution function for the lateral profile and Hermite-Gaussian distribution function for the depth profile. The red-cross dotted curve represents the actual experimental data, while the solid green curve represents the best fit function to the data. The variation of the lateral profile shows a symmetric distribution due to the symmetry in the index distribution of the waveguide in the lateral direction. The variation of the depth profile shows an asymmetric distribution due to large refractive index difference between air above the waveguide and the $LiNbO_3$ substrate below it. The smoothness of the near field profile is an indication of the excellent signal-to-noise ratio obtained when using a stable laser source [19].

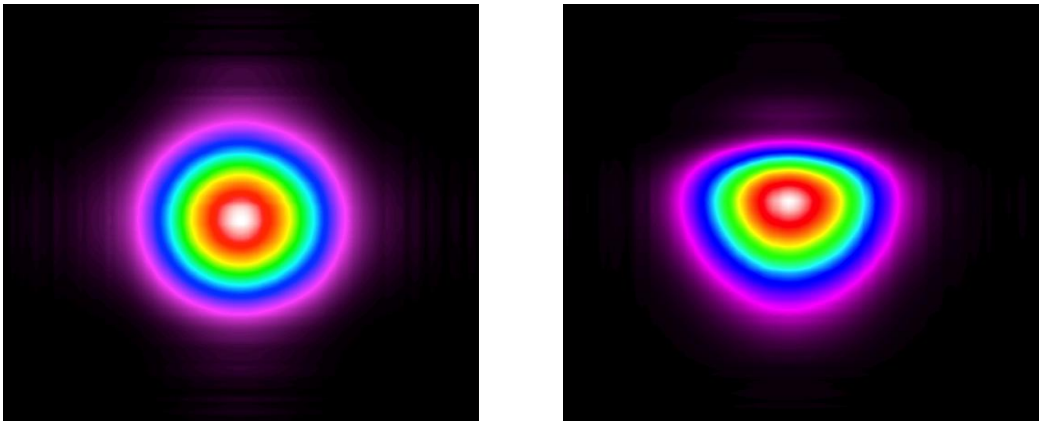

(a) Corning single mode fiber (b) Ti diffused channel waveguide

Fig. 14. Captured images from Thorlabs mode profiler for the input signal of TM input polarization: (a) for a single mode fiber (Corning SMF-28™), (b) for a Ti diffused channel waveguide.

Fig. 14 shows the 2-dimentional contour plots for the output intensity of the single mode fiber (Corning SMF-28™), and 7μm-wide Ti in-diffused waveguide on sample ER21 for transverse magnetic (TM) polarization. As expected, the fiber mode profile has a circular symmetry. On the other hand, the waveguide mode is asymmetric.

The half width at 1/*e* of the intensity profiles was used for the characteristic mode dimensions. According to the measured mode size, coupling efficiency between a single mode fiber and an in-diffused channel waveguide can be calculated from the following overlap integral [19]:

$$\eta = \frac{\left|\int_{-\infty}^{+\infty} \Psi_1(z,x)\,\Psi_2(z,x)\,dz\,dx\right|^2}{\int_{-\infty}^{+\infty}|\Psi_1|^2\,dz\,dx\;\int_{-\infty}^{+\infty}|\Psi_2|^2\,dz\,dx} \tag{36}$$

where Ψ_1 and Ψ_2 are the electric field distributions along the lateral and depth mode profile. The light propagation is along y direction, and x direction is normal to the crystal surface, and z is parallel to the surface.

The electric field distributions are defined as [19]:

$$\Psi_1(z,x) = A_0\,exp(-(z^2 + x^2)/a^2) \tag{37}$$

$$\Psi_2(z,x) = f(z)\cdot g(x) \tag{38}$$

where

$$g(x) = \begin{cases} G_0 \exp(-x^2/\sigma_1^2) \\ G_0 \exp(-x^2/\sigma_2^2) \end{cases}$$

$$f(z) = F_0 \, exp(-z^2/\sigma_3^2)$$

with a is half width at 1/e of the fiber mode intensity profile, σ_1 and σ_2 are the depth parameters and σ_3 is the lateral parameter for the half width at 1/e of the beam mode intensity. The depth parameters σ_1, σ_2, and the lateral parameter σ_3 are illustrated in Fig. 13.

By substituting the equations of (37) and (38) into the overlap integral equation of (36), the coupling efficiency equation reduces to [19]:

$$\eta = \frac{2\left|\left|\frac{1}{a^2}+\frac{1}{{\sigma_1}^2}\right|^{-\frac{1}{2}} + \left|\frac{1}{a^2}+\frac{1}{{\sigma_2}^2}\right|^{-\frac{1}{2}}\right|^2}{a^2\sigma_3(\sigma_1+\sigma_2)\left|\frac{1}{a^2}+\frac{1}{\sigma_3^2}\right|} \tag{39}$$

For the coupling loss calculation, the coupling efficiency needs is expressed in dB $\left(\text{or } 10 \times log(\eta)\right)$. Table 3 shows all the measured half width values at 1/e of the field intensity profile for the transverse magnetic input polarization, the fabrication parameters for the 7μm wide Ti in-diffused straight channel waveguide, and the calculated coupling loss.

The propagation loss (waveguide loss) was obtained by subtracting the coupling loss $(2 \times 0.67\text{dB})$, and Fresnel loss $(2 \times 0.15\text{dB})$ from the measured insertion loss

(3.44dB). The calculated propagation loss for the 39mm long waveguide was 0.46dB/cm for TM polarization, which is acceptable value for a Ti in-diffused waveguide.

Table. 3 Measured field intensity half widths at 1/*e* for 7μm wide straight channel waveguide for the TM input polarization and calculated coupling efficiency and coupling loss

Mode Dimension Parameters of Sample ER21						
Diffusion Parameters	a [μm]	σ_1 [μm]	σ_2 [μm]	σ_3 [μm]	Coupling efficiency	Coupling loss [dB]/side
Temperature = 1025˚ C Thickness = 1070Å Time = 10 hrs Width = 7μm	3.47	3.77	5.22	5.50	0.857	0.67

B. Er-doped Ti Diffused Waveguide Amplifier

The absorption and gain properties of Er-doped Ti-diffused waveguide amplifiers (EDWAs) have been investigated using the measurement setup shown in Fig. 15. The performance of EDWAs was characterized from the spectral output of a broadband light source on the input side of a test sample and an optical spectrum analyzer arrangement at its output side. Amplified spontaneous emission (ASE) light from an Erbium-Doped Fiber (EDF) was used as a broadband source at the 1.55μm regime. The ASE source was assembled in a backward pumping configuration of an EDFA, as illustrated in Fig. 15. The erbium-doped fiber is 5m long and is pumped by a 980nm laser diode (LD), controlled by a current source (ILX Light wave LDX-3207B), through a 980/1550nm WDM coupler.

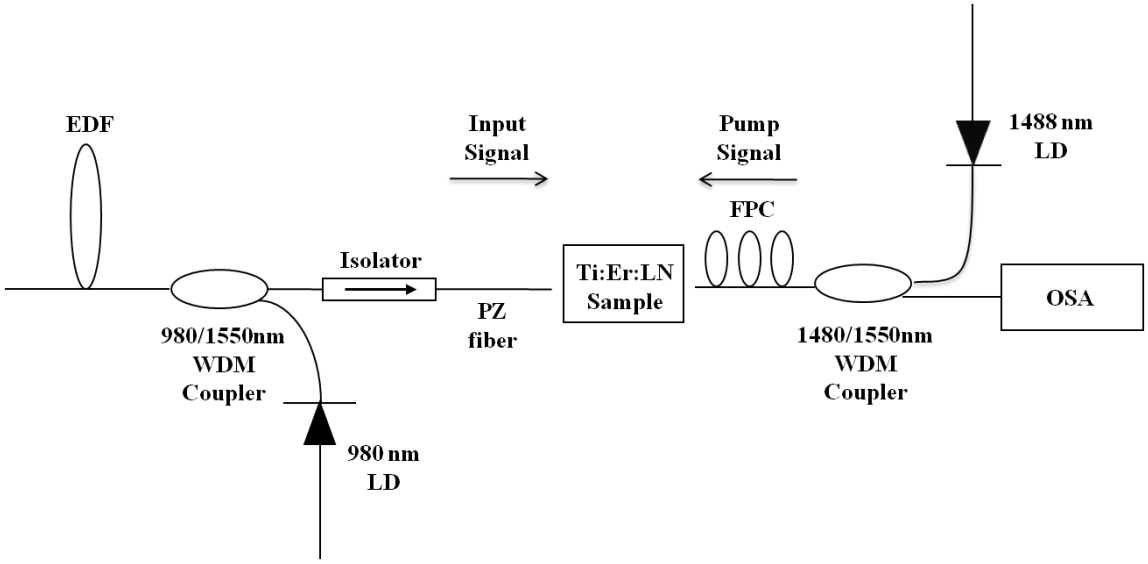

Fig. 15. Experimental setup for the measurement of optical amplification in Ti:Er:$LiNbO_3$

The current source provides a range from 0mA to 200mA. The optical beam was launched through a cleaved polarizing single mode fiber (PZ fiber) by rotating to select Transverse Magnetic (TM) polarization input to the sample. The polarization of the pump signal was selected for TM using a Fiber Polarization Controller (FPC). The pump signal was launched from output facet of the sample using a high power 1488nm Laser Diode (LD), controlled by a current source (ILX Lightwave LDX-3207B), counter-directionally through a 1480/1550nm WDM coupler. The characteristics of the launched 1488nm pump power, to the sample, as a function of pump current is depicted in Fig. 16. The maximum current can be driven up to 500mA which allows maximum launched pump power of 119mW to the sample. The optical spectrum of the amplified output signal was directed through the WDM coupler and displayed on an Optical Spectrum

Analyzer (OSA). Index Matching Liquid (IML) was utilized during the optical characterization.

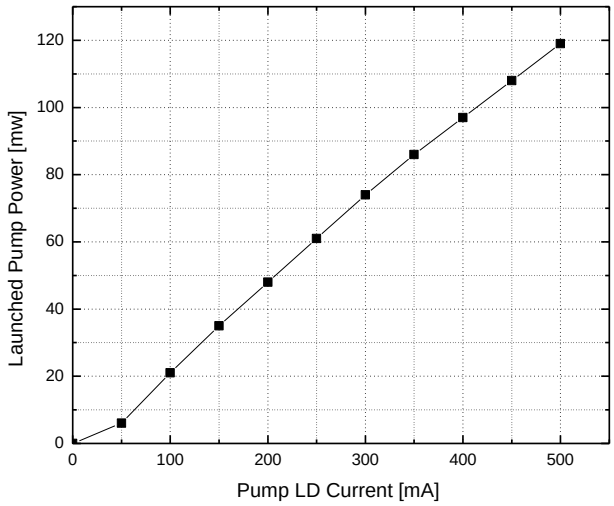

Fig. 16. 1488nm pump power as a function of pump current.

Due to the radiation from excited erbium ions caused by counter-directional 1480nm pumping, an incident input signal can be amplified to compensate for absorption and losses, and eventually reveal gain as the pump power is increased. The amplification is determined by measuring the ratio of the transmitted output signal with pump on-and-off and the net gain is obtained after subtracting the measured absorption spectrum from the amplified signal over the investigated wavelength range [20]. The absorption is maximum when no pump power is applied, and the absorption drops as the pump power increases. When the absorption and waveguide loss are compensated by the increased pump power, gain can be ultimately achieved. The gain saturates with

increasing pump power. The achieved gain may be limited by the maximum available pump power from commercial lasers. The maximum net gain of the output signal at λ_S=1531nm is then calculated using:

$$\begin{aligned} &\textit{Max. Net Gain [dB]} \\ &= \textit{(Output signal level at } P_P = 119\textit{mW of Ti:Er:LiNbO}_3\textit{)} \\ &\quad - \textit{(Output signal level of Ti:LiNbO}_3\textit{)} \end{aligned} \tag{40}$$

The gain was characterized by analyzing the output spectrum at λ = 1531nm as a function of the input pump power level. Small-signal gain characterization was carried out with a -30dBm of transmitted input signal power at λ_S=1531nm, and a 0 to 119mW of counter-directionally launched pump power at λ_P=1488nm. TM polarization was used for both the incident signal and the pump beams. At a maximum launched pump power of 119mW, a signal enhancement of 8.8dBm for 25mm-long erbium doped waveguide amplifier and a signal enhancement of 11.6dBm for 35mm-long erbium doped waveguide amplifier were observed on the optical spectrum analyzer (OSA). The OSA displayed output signal spectrum for non Er-doped Ti in-diffused waveguide is shown in Fig.17. And the output spectrums at different pump power are shown in Figs. 18 to 20 for 35mm-long Er-doped Ti in-diffused waveguide. Maximum net gain values of $Gain_{net}$ = 1.8dB and $Gain_{net}$ = 2.8dB were calculated in 25mm-long and 35mm-long Er-doped waveguide amplifier, respectively.

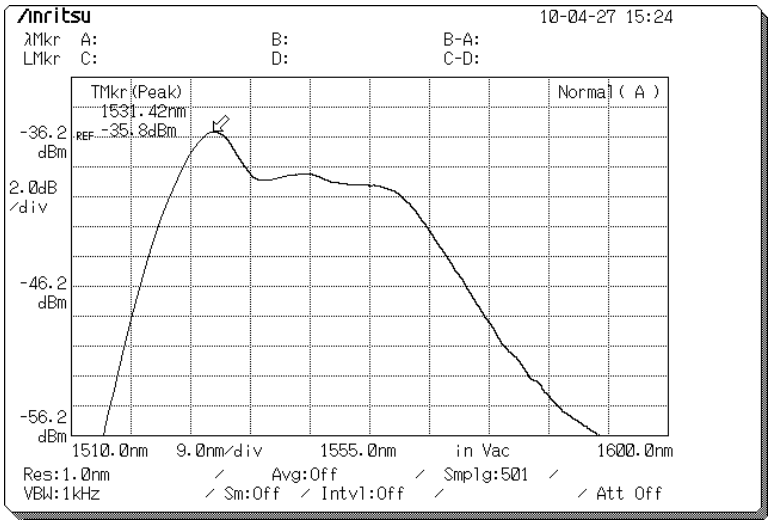

Fig. 17. Signal output spectrum of Ti:$LiNbO_3$ on sample ER21 (39mm long).

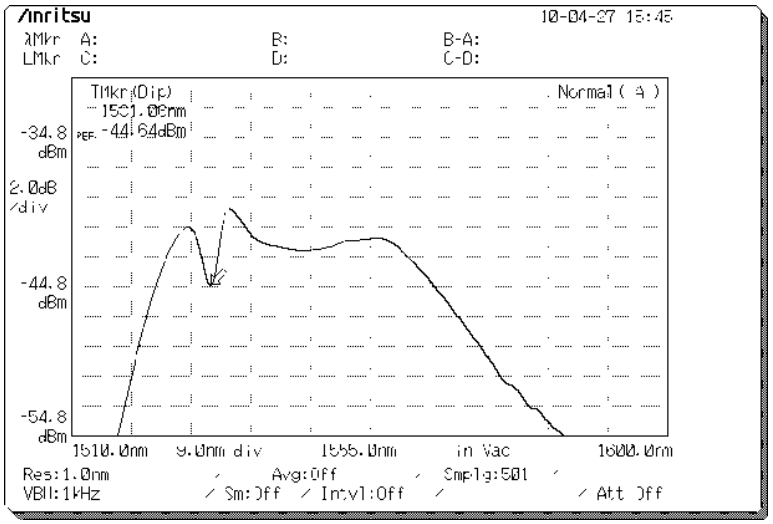

Fig. 18. Signal output spectrum of Ti:Er:$LiNbO_3$ on sample ER21 with $P_P = 0$mW (35mm Er doped region length).

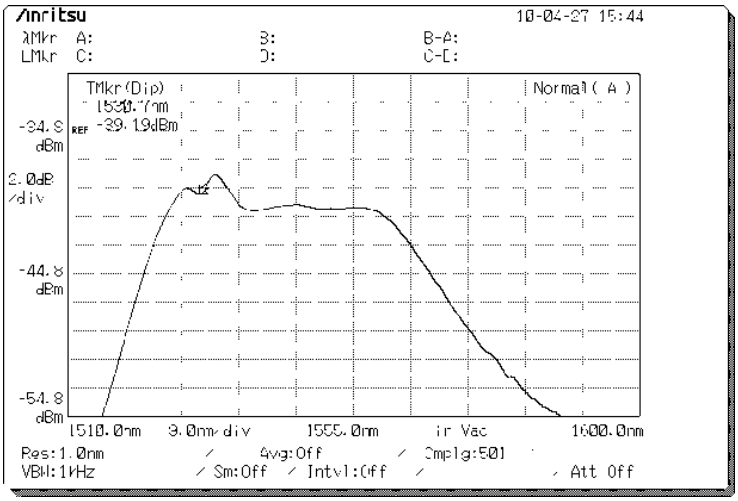

Fig. 19. Signal output spectrum of Ti:Er:$LiNbO_3$ on sample ER21 with P_P=21mW (35mm Er doped region length).

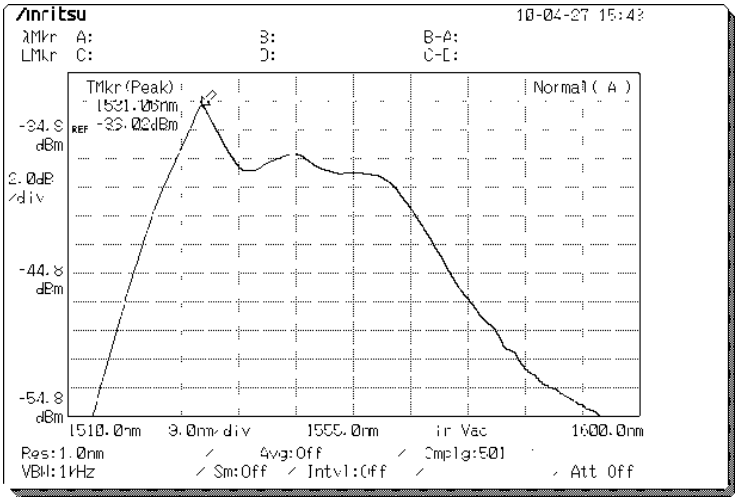

Fig. 20. Signal output spectrum of Ti:Er:$LiNbO_3$ on sample ER21 with P_P=119mW (35mm Er doped region length).

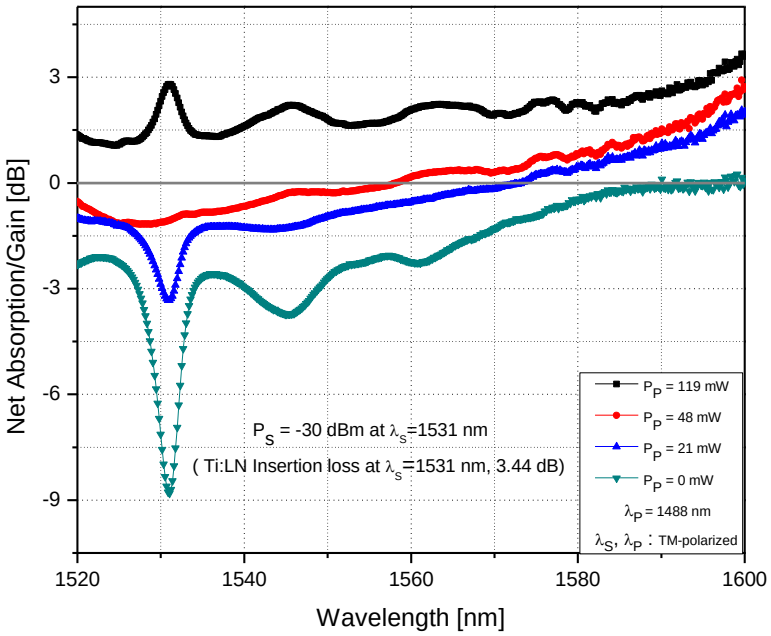

Fig. 21. Measured small signal net absorption/gain in a 35mm-long Er-doped 39mm long Ti diffused $LiNbO_3$ (x-cut) waveguide amplifier on sample ER21 as a function of input signal wavelength at different levels of launched pump power. Both input signal and pump polarization are TM.

Fig. 21 shows the small-signal net absorption/gain output spectra versus different levels of launched pump power. The maximum gain peak of 2.8dB at 1531nm is obtained with the maximum 119mW pump power. The lowest graph represents the absorption spectrum of erbium in Er doped Ti in-diffused $LiNbO_3$ waveguide. With increasing pump power, the absorption and loss are compensated and gain is eventually achieved. The output spectra in Fig. 21 represent the ratio of insertion loss of

Ti:Er:$LiNbO_3$ waveguide relative to non-Er-doped Ti:$LiNbO_3$ waveguide, expressed in dB:

$$Net\ Absorption/Gain\ [dB] = 10 \times log_{10}\left(\frac{\frac{(P_\lambda)_{Ti:Er:LN}}{P_{F-F}}}{\frac{(P_\lambda)_{Ti:LN}}{P_{F-F}}}\right) \qquad (41)$$

where $(P_\lambda)_{Ti:Er:LN}$ is the output signal power of erbium doped titanium in-diffused waveguide at each wavelength, $(P_\lambda)_{Ti:LN}$ is the output signal power of titanium in-diffused waveguide at each wavelength, and $P_{F\text{-}F}$ is the output signal power between input and output fibers without the presence of the sample. All the measured power values were acquired through the OSA.

Fig. 22 shows the variation of the measured small-signal net absorption/gain of the waveguide amplifier as a function of different levels of launched pump power at 1488 nm for an input signal at wavelength λ_S=1531nm. At a launched pump power near 63mW, the absorption and loss are totally compensated. The transmitted signal level at this pump power therefore corresponds to the zero gain level, and the pump intensity is the transparency pump power [2].

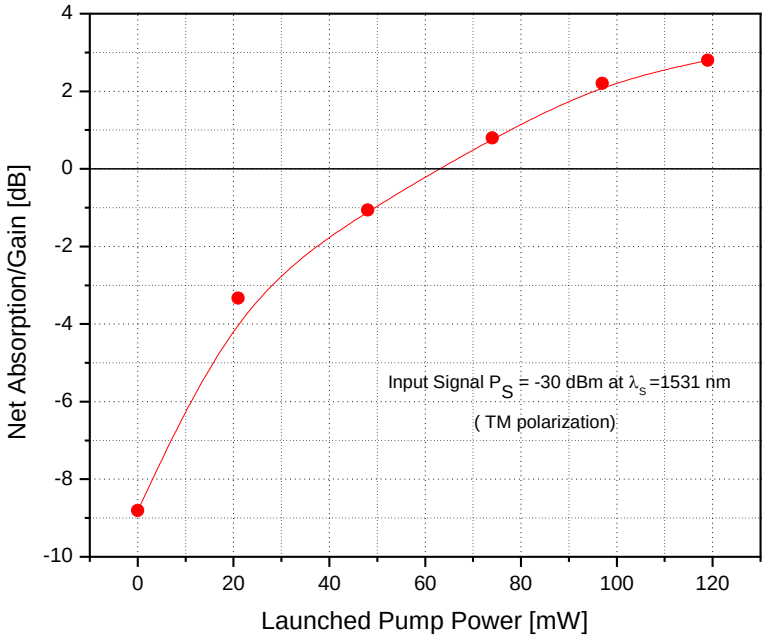

Fig. 22. Measured small signal net absorption/gain of 35mm-long Er-doped 39mm-long Ti diffused $LiNbO_3$ (x-cut) waveguide amplifier on sample ER21 as a function of launched pump power at 1488 nm for an input signal at wavelength λ_S=1531nm. Both input signal and pump polarization are TM.

Fig. 23 shows the expected net gain variation at a launched pump power of 100 mW and 50 mW as a function of input signal power ranging from -30 dBm to 20 dBm at λ_S=1531 nm wavelength. The red circle symbols are experimental data points obtained as the input signal power was varied from -30 dBm to 0 dBm. The blue solid lines represent calculated behaviors reported by Manfred *et al* [13], that are fitted into the measured data points. The trends demonstrate the drop in the rate of gain and saturation.

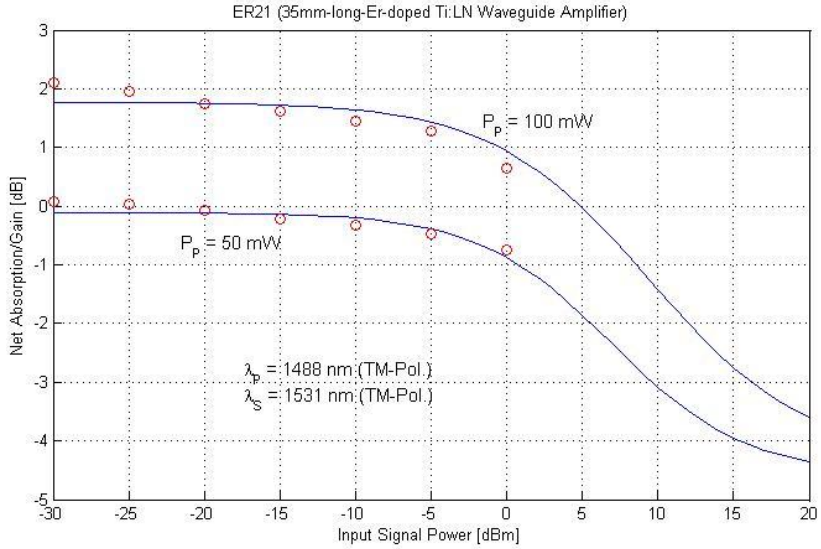

Fig. 23. Measured (red circles) and calculated fitted (blue lines) net gain versus input signal power for two different launched pump powers. Both input signal and pump are TM polarized.

C. Suggestion for Waveguide Amplifier

Possible ways for improving the optical amplification efficiency may be explored by raising the Er diffusion temperature to obtain a deeper dopant distribution, and making the dimension of the selective Er doping region comparable to the waveguide dimension to reduce the absorption. Higher diffusion temperature increases the solubility of Er in $LiNbO_3$ and allows incorporating a considerably larger number of erbium ions within the amplifier structure [21], as well as deeper diffusion depth which would enhance the overlap. Higher concentrations of erbium may also allow the use of shorter length dimensions for the doped regions. However, the diffusion temperature should not exceed Curie temperature of $LiNbO_3$ (~1142˚C), in order to preserve the

single-domain ferroelectric state of the crystal [21] as well as its electrooptic properties. Fig. 24 illustrates a potential alternative configuration. In the research the waveguide width was 7μm, the integration of a narrower width Er region centered on the waveguide will be a challenging task and require extremely accurate alignment controls.

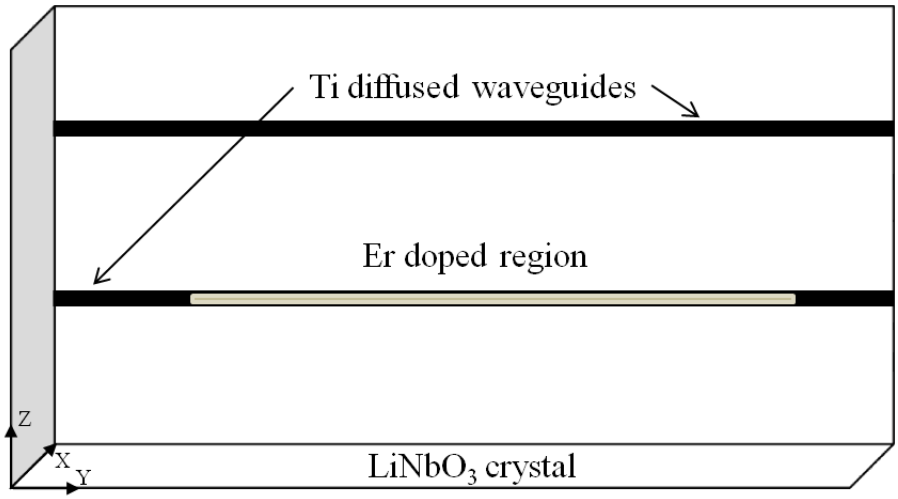

Fig. 24. Suggested alternative configuration.

Another alternative is to use a high-index overlay film as a means to shift the optical fields of the signal and pump beams up toward the surface [22], thus help enhance their overlap with the Er-ions distribution which is concentrated largely near the surface.

CHAPTER V

CONCLUSION

Selectively Er-doped Ti in-diffused $LiNbO_3$ waveguide amplifiers with useful optical gain have been fabricated and characterized. Erbium of suitable thickness was first in-diffused selectively onto the substrate, followed by delineated titanium patterns in-diffusion to form optical waveguides. Optical amplification was demonstrated in the wavelength regime around $\lambda_S = 1.53\mu m$ with counter-directional pumping at $\lambda_P = 1.48\mu m$ wavelength. The performance of the amplifier is based on the interactions between the incident guided optical signal in the $LiNbO_3$ and the evolving emitted radiation from erbium ions excited by the pump beam power.

The Er-doped Ti in-diffused optical waveguide amplifiers were produced on x-cut y-propagating $LiNbO_3$ substrate. The fabrication parameters were optimized to achieve best overlap between the incident guided optical signal mode and evolving Er ions radiation. The selective Er-doping was carried out by diffusing 17nm-thick Er film for 100hours at 1100˚C in photolithographically delineated regions. The optical channel waveguides were formed by diffusing 7μm-wide 1070Å-thick Ti stripes for 10 hours at 1025˚C.

Non-doped Ti diffused optical waveguides were also produced on the same substrate, and were used as reference waveguides. For TM-polarized input, the insertion loss of the reference waveguide was 3.44dB, the measured full width at 1/*e* of the mode

profile was 11.0μm in the lateral direction and 8.99μm in the depth direction, and the propagation loss was 0.46dB/cm.

The characteristics of the optical waveguide amplifiers were investigated using Er-doped fiber as a broadband light source for the input signal. All characterizations were performed using TM polarization. For a 25mm-long Er-doped region, the insertion loss was 10.5dB including Er absorption loss of 7.06dB, and the obtained signal enhancement was 8.8dBm. For a 35mm-long Er-doped region, the insertion loss was 12.26dBm including Er absorption loss of 8.82dB, and the obtained signal enhancement was 11.6dBm. The achieved optical net gain values were 1.8dB and 2.8dB for the 25-mm and 35-mm long Er-doped regions, respectively.

REFERENCES

[1] M. Fleuster, Ch. Buchal, E. Snoeks, A. Polman, "Optical and structural properties of MeV erbium-impanted $LiNbO_3$," *Journal of Applied Physics,* vol. 75, no. 1, pp. 169-172, 1994.

[2] A. Kapoor, G. Jain, E. K. Sharma, "Simplified gain calculation in erbium doped $LiNbo_3$ waveguides," *Proc. Of SPIE,* vol. 6468, 646808, 2007.

[3] J. Amin, B. Dussardier, T. Schweizer, M. Hempstead, "Spectroscopic analysis of Er^{3+} transistion in lithium niobate," *J.Lumi.,* vol. 69, no. 1, pp.17-26, 1996

[4] L. F. Johnson and A. A. Ballman, "Coherent emission from rare earth ions in eletro-optic crystals," *J. Appl. Phys.,* vol. 40, no. 1, pp. 297-302, 1969.

[5] I. Baumann, S. Bosso, R. Brinkmann, R. Corsini, M. Dinand, A. Greiner, K. Schäfer, J. Söshtig, W. Sohler, H. Suche, and R. Wessel, "Er-doped integrated optical devices in $LiNbO_3$," *IEEE J. of Quantum Electronics,* vol. 2, no. 2, pp.355-366 June 1996.

[6] R. Brinkmann, Ch. Buchal, St. Mohr, W. Sohler, and H. Suche, "Annealed erbium-implanted single-mode $LiNbO_3$ waveguides," in *Tech. Dig. Integrated Photonics Research.* Washington, DC: Opt. Soc. Amer., 1990, vol. 5, post-deadline paper PD1.

[7] W. Sohler and H. Suche, "Rare-earth doped lithium niobate waveguide structures," Eur. Patent No. 0 569 353 and U.S. Patent application Serial No. 08 094 199

[8] I. Baumann, R. Brinkmann, Ch. Buchal, M. Dinand, M. Fleuster, H. Holzbrecher, W. Sohler, and H. Suche, "Er-diffused waveguides in $LiNbO_3$," in *Proc. Eur. Conf. Integrated Optics, ECIO'93,* Neuchâtel, Switzerland, 1993, paper 3-14.

[9] A. Yariv, *Quantum Electronics*, 3rd edition. New York: John Wiley & Sons, 1989.

[10] D. K. Cheng, *Field and Wave Electromagnetic*, Reading, MA: Addison-Wesley, Publishing Company, Inc., 1983

[11] R Bansal, *Handbook of Engineering Electromagnetics*, New York: Marcel Dekker 2004

[12] O. Katsunari, *Fundamentals of Optical Waveguides*, 2nd edition. London: Elsevier Inc., 2006

[13] M. Dinand, and W. Sohler, "Theoretical modeling of optical amplification in Er-doped Ti:$LiNbO_3$," *IEEE J. of Quantum Electronics,* vol. 30, no. 5, pp. 1267-1276, May 1994

[14] J. Amin, B. Dussardier, T. Schweizer and M. Hempstead, "Spectroscopic analysis of Er^{3+} transitions lithium niobate," *Journal of Luminescence*, vol. 69, pp.17-26, May 1996

[15] I. Baumann, R. Brinkmann, M. Dinand and W. sohler, "Erbium incorporation in $LiNbO_3$ by diffusion-doping," *Applied Physics A,* vol 64, pp.33-34,1997

[16] F. Caccavale, F. Segato, I. Mansour, J.M. Almeida, and A.P. Leite, "Secondary ion mass spectroscopy study of erbium diffusion in lithium niobate crystal," *Journal of Materials Research*, vol. 13, no. 6, pp. 1672-1678, June 1998

[17] J. L. Jackel, V. Ramaswamy, and S. P. Lyman, "Elimination of out0diffusion surface guiding in titanium-diffused $LiNbO_3$," *Applied Physics Letters,* vol. 38, pp.509-511, Apr.1981

[18] E. L. Wooten, K. M. Kissa, A Yi-yan, E. J. Murphy, D. A. Lafaw, P. F. Hallemeier, D Maack, D. V. Attanasio, D. J. Fritz, G. J. McBrien, and D. E. Bossi, "A review of lithium niobate modulators for fiber-optic communications systems," *IEEE Journal of Selected Topics in Quantum Electronics,* vol. 6, pp.69-82, Jan./Feb. 2000.

[19] P. G. Suchoski, Jr. and R. V. Ramaswamy, "Minimum-mode-size low-loss Ti:$LiNbO_3$ channel waveguides for efficient modulator operation at 1.3μm," *IEEE Journal of Quantum Electronics,* vol. QE-23, no. 10, pp. 1673-1679, October 1987.

[20] K. Wörhoff, J. D. B. Bradley, F. Ay, D. Geskus, T. P. Blauwendraat, and M. Pollnau, "Reliable low-cost fabrication of low-loss Al_2O_3:Er^{3+} waveguides with 5.4-dB optical gain," *IEEE J. of Quantum Electronics,* vol. 45, no. 5, pp. 454-461, May 2009.

[21] R. Brinkmann, I. Baumann, M. Dinand, and W. Sohler, "Erbium-doped single- and double-pass Ti:$LiNbO_3$ waveguide amplifiers," *IEEE J. of Quantum Electronics,* vol. 30, no. 10, pp. 2356-2360, October 1994.

[22] K. Kishioka, T. Kishimoto, and K. Kume, "Improvement of the optical gain in the Er-doped lithium niobate waveguide amplifier,' *IECE Trans electron*, vol. E-88, no. 5, pp.1041-1052, May 2005.

APPENDIX 1

FABRICATION PROCEDURE

1. Dicing $LiNbO_3$ substrate (X-cut, Y-propagating).
2. Clean samples with proper solvents.
3. Image reversal patterning for selective Er film deposition.
4. Vacuum hard bake the image-reversed pattern and O_2 descum.
5. Deposit Er film by DC magnetron sputtering.
6. Lift-off process for delineating the Er regions.
7. Clean the samples with proper solvents.
8. Diffuse the delineated Er regions.
9. Clean the Er-diffused samples with proper solvents.
10. Deposit Ti film by DC sputtering.
11. Delineate waveguide patterns by positive photolithography process.
12. Vacuum hard bake the patterned photoresist.
13. Dry etch Ti film using reactive ion etching (RIE).
14. Wet etch to remove residual Ti using diluted HF acid.
15. Clean the samples using PR stripper and solvents.
16. Diffuse the delineated Ti patterns.
17. Polish the sample end edges to an optical finish.

APPENDIX 2

DICING SUBSTRATE

1. Cut a blue tape in a proper size to put it on O-ring, and place a $LiNbO_3$ on the center of the tape.
2. R Turn on 4 knobs and switched for dicing: water valve, water line valve, air knob under, vacuum pump power switch.
3. **R** Turn on saw power
4. Select PROGRAM 300 and check parameters and confirm to setting..
5. **R** Turn off PROGRAM, and spindle on until blinking light is off.
6. Select ZERO CHECK. Be prepared to push RESET if the blade cuts into chuck.
7. Place the taped O-ring on the chuck, and select WAFER LOCK.
8. Press ALIGN, and align the substrate with crosshairs in eyepiece of microscope using panels on right.
9. Press SINGLE CUT to cut. (Test cut is better required.)
10. When finished, press WAFER RELEASE.
11. Do **R** marked steps in reverse order to shut down machine.
12. Take off diced substrates.

APPENDIX 3

SUBSTRATE CLEANING PROCEDURE

1. Brush a substrate gently with Q-tip in soapy water.
2. Rinse thoroughly with D.I. water.
3. Sonicate in Acetone for 10 minutes
4. Rinse with Methanol.
5. Sonicate in Methanol water for 10 minutes.
6. Rinse with D.I. water.
7. Sonicate in D.I. water for 10 minutes.
8. Rinse with Methanol.
9. Blow dry with N_2.

APPENDIX 4

IMAGE REVERSAL PROCESS

1. Dehydrate samples at 135˚C for 5 minutes in an oven.
2. Wait until samples gets to room temperature.
3. Spincoat Clariant AZ5214 photoresist at 4000rpm for 30 seconds.
4. Softbake (prebake) at 120˚C for 2 minutes.
5. Expose with desired patterned mask at 8.3 mW/cm^2 UV light for 2 seconds without a filter.
6. Postbake at 120˚C for 1 minute..
7. Flood-expose without a mask at 8.3 mW/cm^2 UV light for 1 minute without a filter.
8. Develop samples in a Shipley MF319 for 50 seconds. .
9. Blow dry samples with N_2.

APPENDIX 5

LAYOUT DIMENTION OF SLECTIVE ERBIUM DOPED REGION

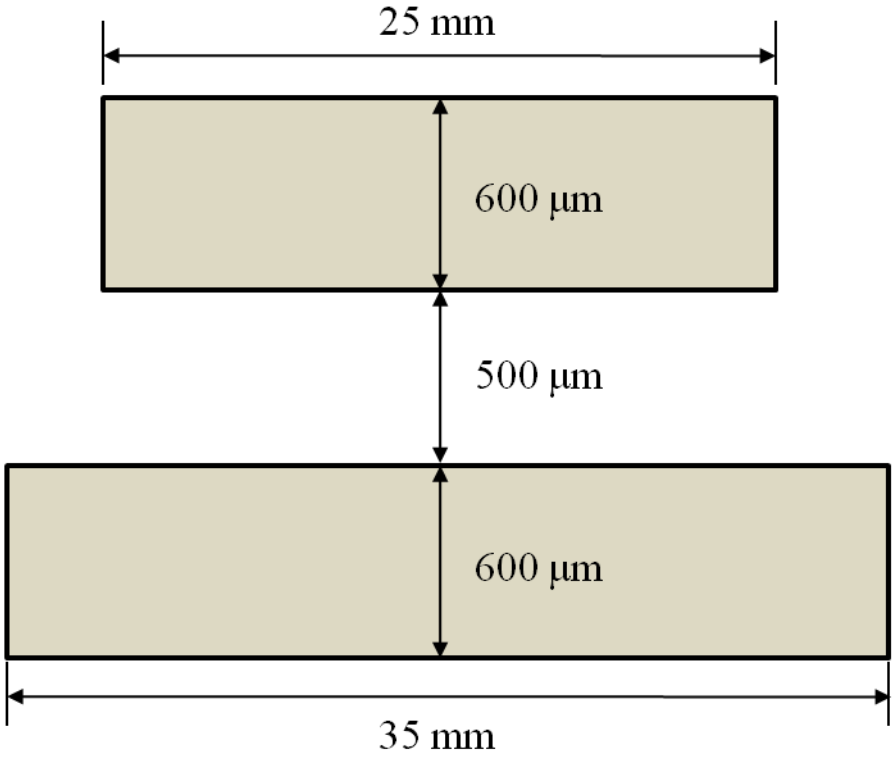

Fig. 25. The mask layout diagram of Er doped region

APPENDIX 6

O_2 PlASMA ASHING AND HARD BAKING

1. Turn on power supply and vacuum pump
2. Vent and load samples into barrel ahser.
3. Pump down a chamber and O_2 line down to a pressure of 50 μmHg.
4. Turn on O_2 valves and adjust flow rate until the chamber pressure reaches 500 μmHg..
5. Turn on FORWARD RF power to 100 watts.
6. Turn RF system to keep reflected power below 5 watss.
7. Run RF for 3 minutes.
8. Turn off the power and O_2 valves.
9. Set temperature 135 ˚C, and hard-bake samples for 15 minutes.
10. Set the temperature below 50 ˚C.
11. Wait until the chamber temperature goes below 50 ˚C.
12. Vent and take out samples, and pump down the chamber for next use.
13. Turn off the power supply.

APPENDIX 7

DC MAGNETRON SPUTTERRING PROCEDURE

1. Vent a chamber, load samples and leave the sample hold not to face Er target.
2. Close a chamber and turn on mechanical pump.
3. Turn on roughing valve, and wait until the chamber gets below 100μmHg..
4. Close the roughing valve and turn off the mechanical pump.
5. Open high vacuum valve all the way.
6. Wait until the chamber pressure drops to below 3×10^{-6} Torr.
7. Turn on coolers for thickness monitor and target holder. (Cooling temperature at 15˚C.)
8. Turn on Argon gas valve and set flow rate at 8sccm.
9. Adjust high vacuum valve for Hasting gauge to reach 5μmHg..
10. Turn on thickness display monitor and set up parameters. (Density: 9.05gm/cc, Z-factor: 0.74, X-tooling: 100%)
11. Turn on power supply and adjust current to be 70mA.
12. Presputter for 15 minutes.
13. Rotate the sample holder for the sample to face Er target for Er deposition.
14. After deposition, adjust current to be 0mA.
15. Turn off the power supply and thickness display monitor.
16. Turn off the Argon flow.
17. Open the high vacuum valve all the way.

18. Wait for more than two hours, and close the high vacuum valve to take out the samples.

APPENDIX 8

ERBIUM IN-DIFFUSION PROCESS

1. Load well cleaned Er-deposited samples on a platinum box, and place it on an alumina tube, and put it in the center of an alumina long tube.
2. Use a quarts rod to push alumina tube to the center of quart tube furnace.
3. Seal the quartz tube with a quart cap at front.
4. Turn on ultra high purity Oxygen valve and adjust flow rate at the backside of the furnace.
5. Set up diffusion temperature at front panel of the furnace.
6. Turn on control switch, and wait until current meters stabilize. Then, turn on element switch.
7. It takes about 1 hour and 25 minutes for the furnace to have the set temperature.
8. Turn off oxygen valve after the time, and turn on ultra high purity Argon valve with a flow rate of 150sccm.
9. When current meter starts to swing on/off, start to count diffusion time.
10. Check the flow rate frequently.
11. After the completion of the diffusion, turn off element and control switches.
12. Change Argon flow to Oxygen flow into the furnace with the same flow rate.
13. After furnace fully cool down, close Oxygen flow and take out alumina tube and samples.

APPENDIX 9

DC SPUTTERING PROCEDURE

1. Turn on TC main power and main power.
2. Vent a chamber, and load samples..
3. Close a bell-jar chamber, and turn on mechanical pump.
4. Turn on roughing valve, and wait until the chamber gets below 100μmHg..
5. Close the roughing valve and turn off the mechanical pump.
6. Open high vacuum valve all the way.
7. Heat bell jar chamber up to 65 ˚C for a couple of hours to dehydrate inside of the chamber.
8. Wait until the temperature drops to the room temperature and also the chamber pressure drops to below 2×10^{-6} Torr.
9. Turn on coolers for thickness monitor and target tray.
10. Turn on Argon gas valve and set flow rate at 140sccm.
11. Adjust high vacuum valve for Hasting gauge to reach 21μmHg..
12. Turn on thickness display monitor and set up parameters. (For Ti, Density: 4.5gm/cc, Z-ratio: 0.628, X-tooling: 325%)
13. Turn on power supply and adjust current knob to be 40mA.
14. Presputter for 15 minutes.
15. Rotate the sample position to start Ti deposition.
16. After deposition, adjust the current knob to be 0mA.

17. Turn off the power supply, thickness display monitor, and Argon gas valve.
18. Open the high vacuum valve all the way.
19. Wait for more than two hours, and close the high vacuum valve to take out the samples.

APPENDIX 10

POSITIVE PHOTOLITHOGRAPHY PROCESS

1. Dehydrate samples at 135 ˚C for 5 minutes in an oven.
2. Leave the samples cool down.
3. Spincoat Clariant AZ5214 phtoresist at 5000rpm for 30 seconds.
4. Soft-bake the samples at 117 ˚C for 2 minutes.
5. Leave the samples cool down.
6. Expose the samples at 11mW/cm^2 UV light for 4.7 seconds without a filter.
7. Develop the samples in a Shipley MF312:H_2O = 1:1.2 solution for 45 seconds.
8. Rinse the samples thoroughly with D.I. water.
9. Blow dry the samples with N_2.

APPENDIX 11

LAYOUT DIMENTION OF WAVEGUIDE PATTERNS ON ERBIUM DOPED AND UN-DOPED REGIONS

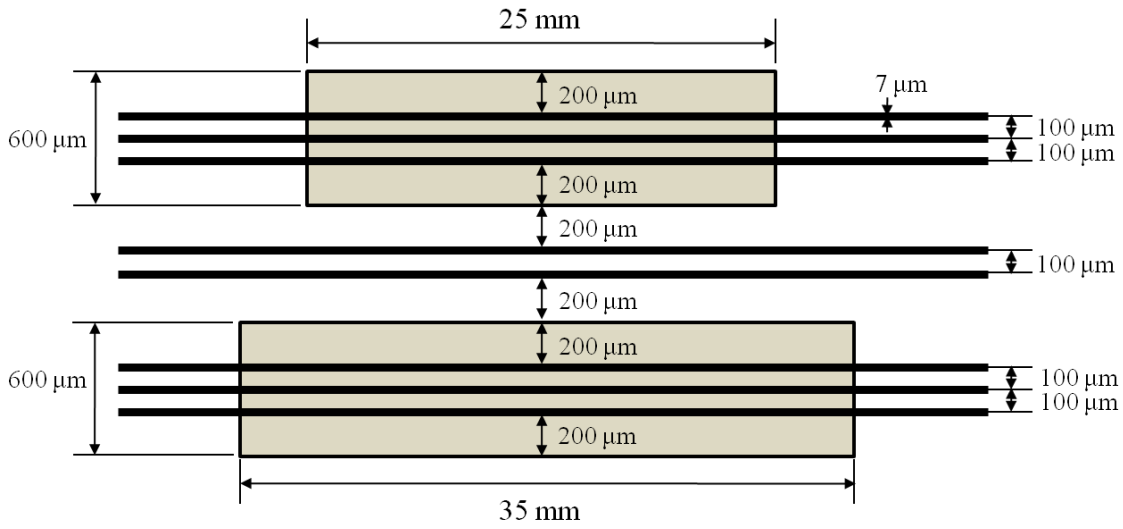

Fig. 26. The mask layout diagram of 7µm-wide straight waveguides in Er-doped regions and un-doped regions.

APPENDIX 12

REACTIVE ION ETCHING (RIE) - OXFORD

1. Turn on power and coolers, and warm up for a while.
2. Check chillers. (Black for turbo and white for RF source)
3. Click VIEW ONLY and long on with ID and Password.
4. Click STOP for load pump, VENT and place samples on a loadlock wafer.
5. Click STOP of mechanical pump and EVACUATE a loadlock chamber.
6. Click PROCESS after getting high vacuum in the chamber.
7. Go RECIPE and LOAD Ti etch.
8. Set up stabilizing time, etching time, and cryo pump temperature as 20˚C.
9. Set up gas flows as CHF_3 ~30sccm, Argon~10sccm, and Helium~10sccm.
10. Set up FORWARD POWER as 100 watts, ICP 600 watts and reflected power below 100 watts.
11. Once it is ready, RUN to start etching.
12. Click VENT and take out sample.

APPENDIX 13

TITANIUM DIFFUSION PROCESS

1. Place well cleaned samples on an alumina tube, and put it in the center of an alumina long tube.
2. Use a quarts rod to push alumina tube to the center of quart tube furnace.
3. Seal the quartz tube with a quart cap at front and connect to a bubbler.
4. Turn on compressed breathing air valve, and adjust flow rate at the backside of the furnace.
5. Set up diffusion temperature at front panel of the furnace.
6. Check the air flow rate of 3 bubbles/second.
7. Turn on control switch, and wait until current meters stabilize. Then, turn on element switch.
8. It takes about 1 hour and 25 minutes for the furnace to reach the set temperature.
9. When current meter starts to swing on/off, start to count diffusion time.
10. Check the flow rate frequently.
11. After the completion of the diffusion, turn off element and control switches.
12. After furnace fully cool down, shut down the air flow and take out alumina tube and samples.

APPENDIX 14

POLISHING PROCESS

1. Place a sample into a polishing mount and secure the mount to a polishing jig.
2. Flow water on the polishing chuck.
3. Put on s sand paper on the chuck.
4. Start rough polishing at 7rpm.
5. Put away the sand paper and put on a 15µm diamond polishing grit paper.
6. Start polishing at 7rpm.
7. Put away the sand paper and put on a 3µm diamond polishing grit paper.
8. Start polishing at 5rpm.
9. Put away the sand paper and put on a 0.5µm diamond polishing grit paper.
10. Start polishing at 3rpm.
11. Put away the sand paper and put on a 0.3µm diamond polishing grit paper.
12. Start polishing at 3rpm.
13. Take out the sample out of the mount and clean it.
14. Inspect edge quality under microscope before optical test.

VITA

JaeWoo Suh was born in Kangjin, Korea. He received his B.S. degree in electrical engineering from Texas A&M University, USA in 2007. He started his master's program in electrical engineering at Texas A&M University in August 2007 and received his M.S. degree in December 2010. He can be reached at the following address:

JaeWoo Suh

Department of Electrical Engineering
c/o Dr. Ohannes Eknoyan
Texas A&M University
College Station, TX 77843-3128